UNIVERSITY OF OKLAHOMA

GRADUATE COLLEGE

IMPACTS OF EXTRATROPICAL TRANSITION ON TROPICAL CYCLONE TORNADO OCCURRENCE

A THESIS

SUBMITTED TO THE GRADUATE FACULTY

in partial fulfillment of the requirements for the

Degree of

MASTER OF SCIENCE

By

KAYLA WHEELER

Norman, Oklahoma

2023

Downloaded from SHAREOK. Persistent Handle URL: https://hdl.handle.net/11244/337933

IMPACTS OF EXTRATROPICAL TRANSITION ON TROPICAL CYCLONE TORNADO OCCURRENCE

A THESIS APPROVED FOR THE
SCHOOL OF METEOROLOGY

BY THE COMMITTEE CONSISTING OF

Dr. Benjamin Schenkel (Co-Chair)

Dr. Nusrat Yussouf (Co-Chair)

Dr. Jason Furtado

Dr. James Ruppert

© Copyright by KAYLA WHEELER 2023
All Rights Reserved.

Acknowledgments

I would like to thank many people that helped me complete this project. My advisors, Dr. Benjamin Schenkel and Dr. Nusrat Yussouf, have been very helpful and supportive every single step of the way and I can't be more grateful. I'm so excited to be pursuing my Ph.D. with them over the next few years. I would also like to acknowledge our grant, NSF AGS-2028151. Next, I would like to thank my committee members, Dr. Jason Furtado and Dr. James Ruppert. Their advice and insight has been invaluable. I would also like to thank Roger Edwards for sharing his knowledge on TC tornadoes and giving advice.

I wouldn't be here without my family's support and advice and I am very grateful. I'd also like to thank my friends from home and that I met here at OU that have supported me throughout this process and helped keep my life balanced with fun! Finally I would like to thank my partner and father of my 2 guinea pigs, Ty, for always being there for me when I've needed it and helping me in any way that I needed.

Table of Contents

Acknowledgments **iv**

List Of Tables **vi**

List Of Figures **vii**

Abstract **ix**

1 Introduction **1**

2 Data & Methods **7**
2.1 TC and Tornado Data 7
2.2 Reanalysis Data 7
2.3 Extratropical Transition Definition 8
2.4 Vertical Wind Shear 11
2.5 Radiosonde Data 12
2.6 Statistical Testing 15

3 Tornado and TC Characteristics **17**
3.1 Tornado Location 17
3.2 Tornado Timing, Frequency, and Damage 23
3.3 Characteristics of the TC and Its Synoptic-Scale Environment 26

4 TC Convective-scale Environments **32**
4.1 Thermodynamic Characteristics 32
4.2 Kinematic Characteristics 37

5 Summary and Discussion **41**

Reference List **47**

List Of Tables

2.1 Number of tornadoes and radiosondes sorted by transition phase in this study. 13

List Of Figures

2.1 Heat map showing radiosonde location plotted in VWS-relative coordinates and with respect to the TC center. 14

3.1 Heat map showing the location of tornado occurrence in the United States for (a) tropical, (b) transition, and (c) extratropical phase tornadoes. 20

3.2 Heat map showing TC-relative tornado location plotted in North-relative coordinates and with respect to TC center for (a) tropical, (b) transition, and (c) extratropical phase tornadoes. Dashed gray lines represent range rings in 100 km intervals from the TC center. 21

3.3 As in Figure 3.2, except plotted in VWS-relative coordinates. The VWS vector (gray arrow) has been rotated to always point to the right of the plot, with tornadoes rotated by the same angle. 22

3.4 Histogram of percent of tornadoes observed binned by local standard time in the tropical phase (pink), transition phase (purple), and extratropical phase (blue). Black error bars show the 95% confidence interval computed using a 5,000 bootstrap resampling approach with replacement. 23

3.5 As in Figure 3.4, except showing number of tornadoes per 6-h with the y-axis using a logarithmic scale. Only periods when the TC was over land were considered. 6-h temporal resolution shown due to Best-Track TC dataset having this resolution. 24

3.6 As in Figure 3.4, except showing tornado damage ratings. 25

3.7 As in Figure 3.4, except showing TC intensity as the Best-Track maximum 10-m wind speed (kt) interpolated to the time of tornado occurrence. 27

3.8 As in Figure 3.4, except showing TC near-surface outer wind field size as the radius at which the azimuthal-mean 925-hPa azimuthal wind equals 6 m s^{-1} (r_6; km), calculated from the ERA-5 reanalysis, interpolated to the time of tornado occurrence. 28

3.9 As in Figure 3.4, except showing interpolated VWS magnitude (m s^{-1}) to the time of tornado occurrence. 31

3.10 As in Figure 3.4, except showing interpolated 850–200-hPa VWS direction to the time of tornado occurrence. 31

4.1 Box-and-whiskers plots of 0–3-km CAPE (J kg^{-1}) values across phases and VWS-relative quadrants. The box perimeter shows the interquartile range. The line across the middle indicates the median, while the notches represent the 95% confidence interval of the median. Whiskers extend from both the bottom of the box (25th percentile) to the lowest observed datum and from the top of the box (75th percentile) to 1.5x the interquartile range. Diamonds indicate outliers. 34
4.2 As in Figure 4.1, except for CIN (J kg^{-1}) up to 500-hPa. Some outliers are excluded from this figure to more clearly highlight the middle of the distribution. 35
4.3 Composite median skew T–log$P$ diagrams for the (a) upshear left, (b) upshear right, (c) downshear left, and (d) downshear right quadrants in the tropical (dark pink), transition (purple), and extratropical (blue) phases. Temperature is illustrated by the solid lines and dashdot lines represent dewpoint. 36
4.4 As in Figure 4.1, but for 0–3-km SRH (m^2 s^{-2}). Note that whiskers in this figure extend from the box edges to 1.5x the interquartile range in both directions. 38
4.5 Composite median hodographs for the (a) upshear left, (b) downshear left, (c) upshear right, and (d) downshear right quadrants in the tropical, transition, and extratropical phases for transitioning TCs. TC motion has been removed from each radiosonde in an attempt to isolate changes in TC winds. Stars represent composite median Bunkers storm motion vector for each phase in each VWS-relative quadrant. Dashed rings are shown at 5-m s^{-1} intervals. Black circles of different sizes show winds at the surface (i.e., typically below 10 m), 1-km, 3-km, and 6-km heights. Note: All three phases begin with weakly cyclonic or even anticyclonic inflow winds in the downshear right quadrant, similar to previous work (Baker et al. 2009). 40

Abstract

Tornadoes that spawn from tropical cyclones (TCs) pose a threat to lives and property. While nearly half of TCs in the Atlantic Ocean undergo extratropical transition, there has only been one study investigating how tornado occurrence changes during transition. The present study conducts a climatological analysis of the impact of extratropical transition on tornado occurrence in TCs from 1995–2020 by utilizing both observed TC and tornado data as well as radiosonde data. This study broke extratropical transition into three phases: tropical (i.e., pre-transition), transition, and extratropical (i.e., post-transition). The tropical phase and transition phase tornadoes have the largest portion of tornadoes analyzed in this study as well as the highest frequencies of tornadoes, while the extratropical phase has the fewest and least frequent tornadoes. Analysis of tornado location showed that tornadoes occur increasingly north and east as transition progresses, associated with the recurvature of TCs into the midlatitudes. Further analysis showed that as transition progresses, tornadoes tend to shift farther south within the TC, occur later in the day, and are associated with greater damage. These changes in tornado characteristics are associated with increases in synoptic-scale deep-tropospheric vertical wind shear, whilst TC intensity weakened and the extent of the outer wind field expanded. Evaluation of radiosondes showed that the downshear right quadrant of the TC is frequently the most favorable for tornado production, having the highest CAPE, lowest CIN, and highest storm-relative helicity (SRH) values. Throughout transition, CAPE in the downshear right quadrant decreases and CIN has no significant changes. SRH in this quadrant increases at the beginning of transition and decreases following transition. In all quadrants, CAPE tended to decrease as the lower tropospheric became cooler and drier in all quadrants due to transition, although those to the left-of-shear experienced this cooling much sooner than right-of-shear. SRH tends to increase, by varying magnitudes by quadrant, as transition begins associate with lower-tropospheric wind increases that are associated with stronger lower-tropospheric vertical wind shear followed by either a decrease or no significant change following transition.

Chapter 1

Introduction

Tropical cyclones (TCs) produce tornadoes in addition to many other hazards such as storm surge, flooding, and strong winds. A climatology for TC tornadoes has been established that focuses on the timing, location, and frequency of tornadoes as well as the factors that determine these characteristics. In the studies that contributed to the climatology, the entire life of a TC was considered (McCaul 1991; Edwards 2012). According to the climatology, tornadoes tend to occur in the northeast quadrant of the cyclone at approximately 100–500-km from the center (Novlan and Gray 1974; McCaul 1991; Schultz and Cecil 2009). As radial distance from the center of a cyclone increases, the amount of convective available potential energy (CAPE) typically increases, which can cause supercells to become more prevalent (McCaul 1991). Supercells within TCs have shallower mesocyclones (i.e., low-topped or miniature supercells) and are weaker than the typical supercells that occur in the Great Plains (McCaul and Weisman 1996). These weaker supercells tend to produce less damaging tornadoes, having 93% causing light-to-moderate damage with Enhanced Fujita (EF) Scale EF/F0 to EF/F1 tornado damage ratings (Edwards 2012; Edwards and Mosier 2022). However, due to poor visibility and multiple concurrent hazards (e.g. heavy rainfall) during a TC, tornadoes can be hard to spot and damage difficult to distinguish (Edwards 2012).

The climatology of TC tornadoes also indicates patterns in the timing of tornado occurrence. Most tornadoes occur within the 48 hours before and after landfall (McCaul 1991). Additionally, TC tornadoes tend to follow a diurnal cycle with the greatest number of tornadoes occurring during the afternoon and evening from 1100

to 1800 local standard time (LST) (Schultz and Cecil 2009). This distinct maximum of tornadoes in the daylight hours may be partially due to better visibility during the day making it easier to see tornadoes or that CAPE is maximized during the daytime, making conditions more favorable for tornadic activity (McCaul and Weisman 1996). The greatest proportion of strongly damaging TC tornadoes occur during the nighttime hours from 0300 to 0900 UTC (Edwards 2012).

While an extensive climatology has been developed for TC tornadoes, little research has been done to examine changes in tornado occurrence during the process of extratropical transition. Klein et al. (2000) and Evans et al. (2017) describe extratropical transition as the structural changes that a TC undergoes upon moving over an area with lower sea surface temperatures (SSTs) and into a baroclinic zone. The entire transition typically takes about two days (Klein et al. 2000). Forty-two percent of Atlantic TCs undergo extratropical transition (Hart and Evans 2001). Due to the common occurrence of this process, an understanding needs to be developed of how, if at all, extratropical transition impacts the occurrences of hazards such as tornadoes.

In order to understand how extratropical transition may impact tornado occurrence, the process itself must be understood. According to the climatology described by Klein et al. (2000); Evans et al. (2017), extratropical transition begins once the outer circulation of a warm-core TC begins to interact with a baroclinic zone and the TC moves over cooler SSTs or over land. The TC begins to weaken due to the decreased SSTs. As it interacts with the baroclinic zone, the tangential winds advect warm, moist air poleward along the east side of the cyclone that result in deep convection. Along the west side of the cyclone, cold and dry air is advected equatorward which becomes warmed and moistened and produces shallow cumulus clouds in the stable air mass. The two different cloud structures on either side of the TC cause its structure to take on an asymmetrical shape. Exposure to increased synoptic-scale,

deep-tropospheric vertical wind shear (VWS) in association with an upstream upper-tropospheric trough further enhances the asymmetry. This VWS displaces the cirrus shield of the TC downshear (i.e. to the side of the TC relative to the direction of the VWS vector) of the cyclone. These aspects of cyclone shape change are early indicators that extratropical transition has begun (Klein et al. 2000; Evans et al. 2017).

As the TC progresses farther into the baroclinic zone, the continued temperature advection causes warm and cold conveyor belts to form (Klein et al. 2000; Evans et al. 2017). These conveyor belts change the orientation of the baroclinic zone from zonal to a southwest to northeast orientation. The air from the warm conveyor belt moves along the east side of the cyclone and ascends over the tilted isentropic surfaces. A portion of air parcels from the warm conveyor belt are then moved cyclonically with the primary circulation of the cyclone and descend along the west side. This results in a dipole of vertical motion on either side of the TC of rising motion to the east and sinking motion to the west (Klein et al. 2000; Evans et al. 2017). VWS further increases as the TC becomes confluent with the approaching upper-tropospheric trough. The increased VWS yields ascent, saturation, and strong convection in the downshear portion of the cyclone with suppressed convection upshear (i.e. side of TC opposite of direction of VWS vector) (Klein et al. 2000; Evans et al. 2017). The downshear portion of the TC experiences enhanced veering, which enhances the secondary circulation, further contributing to the asymmetry of the wind field of the cyclone (Franklin et al. 1993; Black et al. 2002; Molinari and Vollaro 2008). The polar jet interacts with the cyclone by advecting cold and dry air and "ventilating" the TC, weakening the TC warm core as the upper-tropospheric part is eroded and advected downshear and tilts the vortex. This "ventilation" results in the erosion of convection upshear as well, further diminishing convection along that portion of the TC (Jones 1995; Tang and Emanuel 2010).

These processes associated with the conveyor belts and the increasing VWS continue as the TC fully embeds itself into the baroclinic zone. The upper-tropospheric part of the warm core continues to erode into a weaker lower tropospheric warm core and finally, in most cases, becomes a cold-core cyclone(Klein et al. 2000). Occasionally, there are cases where the TC retains the warm core and becomes what is called a warm-seclusion extratropical cyclone (Shapiro and Keyser 1990). Erosion of the south and west parts of the eye wall occur as the descent of air parcels along the west section of the TC continues (Klein et al. 2000). Warm and cold fronts form from the conveyor belts and the cyclone becomes strongly frontal. The source of energy for the cyclone shifts from heat flux by warm SSTs to that of a typical midlatitude cyclone, baroclinic processes. Extratropical transition is considered completed once the TC takes on a structure with a thick layered band of clouds on the poleward side indicating the warm front and a weaker band of clouds in the southeast quadrant indicating the cold front (Klein et al. 2000; Evans et al. 2017).

One method that is applied to diagnose extratropical transition in model and reanalysis datasets is the Cyclone Phase Space, which is used operationally to help diagnose the beginning and end of transition (Hart 2003). The Cyclone Phase Space parameters measure the change in geopotential height field with height and the difference in thickness between the directionally-determined left and right sides of the cyclone. These two parameters provide insight into what phase of extratropical transition is in by showing the type of core the cyclone has and how symmetrical the wind field is. Due to its simple and efficient means of diagnosing TC phase, the Cyclone Phase Space method was selected for this study.

As mentioned previously, past studies of TC tornadoes have included all phases of the life of a TC, but have yet to distinguish tornado occurrence between the phases of extratropical transition. To common knowledge, only one prior study, Hill et al. (1966), has done an analysis of TC tornadoes while considering extratropical transition. This study showed that most tornadoes occurred in the southeast quadrant

of the TC following the end of extratropical transition. Tornadoes occurring directly to the east of the center were mostly within 260 km of the center while tornadoes to the south of the center were more spread out within 555 km. This pattern differs from previous studies that show that most tornadoes occurred in the northeast quadrant (Novlan and Gray 1974; McCaul 1991; Edwards 2012). This shows that the results of this 1966 study need to be revisited and expanded upon using modern observations (e.g. WSR-88D), warning, and verification practices. Analysis of additional aspects of tornado occurrence including timing and frequency through extratropical transition has yet to be performed and can be with the use of the aforementioned modern practices.

This study was conducted to fill the gap in knowledge regarding TC tornado occurrence during the process of extratropical transition. Before beginning the process, it was hypothesized that the process of extratropical transition causes asymmetries in TC structure that affect the synoptic-scale environment and TC characteristics, which impact the convective-scale environments, and thus impacts TC tornado occurrence. The primary scientific objectives of this study are as follows: 1) Establish a climatology of TC tornado location, timing, and frequency before, during, and after transition and 2) analyze radiosonde data to understand what convective-scale environmental changes in association with transition. To complete these objectives, the Cyclone Phase Space method is utilized to distinguish timesteps during a TC into three phases: tropical, transitioning (referred to as "transition"), and extratropical. Comparison was then performed between these three phases with regard to characteristics of tornadoes and TCs. Radiosonde data was then analyzed to compare environments between the three phases during tornadic periods. Throughout this process, the following questions were considered:

1. Does the location, timing, frequency, or damage rating of TC tornadoes change as the TC undergoes extratropical transition?

2. How do synoptic-scale characteristics of the TC that could impact tornado occurrence change as the TC undergoes extratropical transition?

3. How do the convective-scale environments in which TC tornadoes are produced change as the TC undergoes extratropical transition?

Chapter 2

Data & Methods

2.1 TC and Tornado Data

Atlantic TC location and intensity were obtained from the 6-h National Hurricane Center (NHC) Best-Track data from 1995–2020 (Landsea and Franklin 2013). All TCs in the Best-Track were tracked until their dissipation or absorption into a baroclinic zone or larger extratropical cyclone.

The Best-Track dataset was used to construct the Storm Prediction Center TC tornado (TCTOR) data which contains TC tornado track, initial time of tornado occurrence, and damage ratings from 1995–2020 (Edwards and Mosier 2022). The initial time of tornado track was used in this analysis. The utilized time period corresponds with the widespread use of WSR-88D radar data and modernization of warning and verification processes, making this data more reliable compared to prior years (Spratt et al. 1997; Edwards and Mosier 2022). Only those TCs that both completed transition according to the Best-Track dataset and produced at least one tornado according to the TCTOR dataset were considered. These criteria yield 58 TCs that were initially considered.

2.2 Reanalysis Data

This study used geopotential height, vector wind data, and mean sea-level pressure (MSLP) from the European Centre for Medium Range Forecasts fifth-generation reanalysis (ERA5; Hersbach et al. 2020). ERA5 data is 6-hourly and on a $0.25^\circ \times 0.25^\circ$

grid. ERA5 has been used to compute the parameters in Cyclone Phase Space in prior work (Sarro and Evans 2022).

Due to the nontrivial uncertainties in determining TC center location in observations and reanalysis data, vortex recentering was performed to identify the center of the TC (Schenkel and Hart 2012; Torn and Snyder 2012; Hodges et al. 2017). First, the Best-Track-defined center was used as an initial guess for center location. Then, the reanalysis center was calculated as the mean of the center of mass of MSLP as well as 925, 850, and 700-hPa relative vorticity, and 850 and 700-hPa geopotential height. This method has been used in prior work and is similar to the Geophysical Fluid Dynamics Laboratory (GFDL) operational tracker (Marchok 2002; Brammer and Thorncroft 2017; Schenkel et al. 2017). The objectively-tracked TC center was used in determining phases of extratropical transition as well as calculating VWS.

2.3 Extratropical Transition Definition

While the Best-Track dataset provided the time that extratropical transition ends, the start of transition was also required to demarcate the boundary between the tropical (i.e., pre-transition) and transition phases. Thus, the Cyclone Phase Space method was utilized in this study to objectively define the start and end of extratropical transition (Hart 2003). The Cyclone Phase Space (hereafter referred to as "phase space") uses three parameters to categorize cyclones: the lower-tropospheric (900–600-hPa) thermal asymmetry (B), the lower-tropospheric thermal wind (-V_T^L), and the upper-tropospheric (600–300-hPa) thermal wind parameters (-V_T^U). Two of these parameters, the thermal asymmetry and lower-tropospheric thermal wind parameters are used to define the start and end of transition.

The thermal asymmetry parameter is defined as the difference in lower-tropospheric layer fields on either side of cyclone motion and is calculated using the following equation:

$$B = h(\overline{Z_{600hPa} - Z_{900hPa}}|_R - \overline{Z_{600hPa} - Z_{900hPa}}|_L) \tag{2.1}$$

It is useful in determining if a TC has lost its symmetric structure that is typically present in the tropical phase and has become frontal (Hart 2003; Evans and Hart 2003). This parameter is computed as the difference in lower-tropospheric height thicknesses between the left and right sides of TC motion averaged across a 500-km radius from the objectively-tracked TC center from 900-hPa to 600-hPa. In the Northern Hemisphere, a positive thermal asymmetry value indicates that the side to the right of the cyclone motion vector has deeper lower-tropospheric thicknesses, meaning the right side is warmer and moister than the left side of the TC. A negative thermal asymmetry value indicates that the layer thicknesses to the left of the cyclone motion vector are warmer and more moist than the right. When the thermal asymmetry is greater than an empirically defined value of 10-m while the TC is warm core, the storm has become sufficiently frontal to classify it as a transitioning cyclone (Hart 2003; Evans and Hart 2003).

The lower-tropospheric thermal wind parameter characterizes the lower-tropospheric vertical structure of the cyclone by measuring how the isobaric height gradient of the TC changes with height (Hart 2003). This is calculated using the following equation:

$$(\Delta Z)(\ln p)\Big|_{900hPa}^{600hPa} = -|V_T^L| \tag{2.2}$$

If the height gradient and winds of the cyclone increase with height ($-V_T^L < 0$), then the cyclone is classified as cold core. Oppositely, if the height gradient and winds that decrease with height ($-V_T^L > 0$), the cyclone is classified as warm core. To calculate the phase space parameters, heights between 900–600-hPa within a 500-km radius of the objectively-tracked TC center were obtained from ERA5. Extratropical transition was defined to end when the cyclone is frontal (thermal asymmetry parameter magnitude greater than 10m) and the height gradient and winds increase

with height (negative thermal wind parameter). Additionally, a 24-h running mean was applied when calculating the thermal symmetry and thermal wind parameters, following prior work (Hart 2003; Hart et al. 2006).

Using phase space methodology, the life of each extratropically transitioning TC was divided into three phases (Hart 2003; Evans and Hart 2003): 1. tropical (i.e., pre-transition), 2. transition, and 3. extratropical (i.e., post-transition). The tropical phase includes 6-h track timesteps in which the outer rainbands of the TC overlap with the continental United States and the TC itself is considered non-frontal ($B <$ 10 m) and warm core ($-V_T^L > 0$). The transition phase includes 6-h timesteps in which the TC is considered frontal ($B >$ 10 m) and warm-core. The final phase, extratropical, can take two different forms. The most frequent form is when the cyclone immediately becomes cold-core ($-V_T^L < 0$) and frontal. The other, warm-seclusion, is when the cyclone remains a warm core and frontal cyclone, but has concluded the process of transitioning (Hart et al. 2006; Sarro and Evans 2022).

Additional steps had to be taken for TCs in which phase space did not accurately represent the process of transition. Some TCs had differences of more than 18 hours between the Best-Track-determined end of extratropical transition and the end of transition determined by phase space. The 9 TCs where this difference occurred were excluded from this study due to unrealistic representation of extratropical transition in the reanalysis, following Sarro and Evans (2022). Additionally, warm-seclusion extratropical cyclones pose a known issue for phase space as they maintain a warm-core as an extratropical cyclone, which phase space would falsely identify as still being a transitioning TC. Also following Sarro and Evans (2022), the Best-Track time of transition end is selected instead of the phase space time for the 11 cyclones that have been subjectively identified as having transitioned into warm-seclusion extratropical cyclones. To identify these cases, all TCs that remained warm core and frontal for at least 18 hours after Best-Track-determined transition were selected for further

investigation. This was done by subjectively verifying frontal structure by using reanalysis data (e.g., 700-hPa frontogenesis) and verifying extratropical cyclone cloud structure (e.g., asymmetric (frontal) distribution and a cirrus shield (Klein et al. 2000)) in observed satellite imagery following the methodology from Sarro and Evans (2022). In other cases, there were multiple parts of the lifespan of a TC that met the criteria for being classified as a "transition" period. As an example, some TCs had baroclinic origins, causing them to have an asymmetrical shape with a warm core at the very beginning of their life (Davis and Bosart 2004; McTaggart-Cowan et al. 2008). For TCs with this atypical life cycle, the transition period within 18-h of Best-Track end-of-transition time was manually selected. All other TCs underwent extratropical transition in the expected manner, meaning that they progressed from the tropical to transition to the extratropical phase and ended as a cold-core and frontal cyclone (Hart et al. 2006; Sarro and Evans 2022).

Table 2.1 shows the number of tornadoes in each of the three phases associated with extratropical transition.

2.4 Vertical Wind Shear

Prior work has found that VWS strongly impacts the location and number of tornadoes, inspiring the analysis of this study to often use a VWS-relative framework (Schenkel et al. 2020, 2021). VWS is calculated following methodology from previous studies (Davis et al. 2008; Galarneau and Davis 2013; Rios-Berrios and Torn 2017): 1) compute the irrotational and nondivergent wind components within 500-km of the TC at 850-hPa and 200-hPa by solving a Poisson equation with homogeneous boundary conditions, 2) subtract those wind components from the total wind field at both pressure levels to isolate the ambient winds, and 3) subtract the 850-hPa ambient winds from the 200-hPa ambient winds. Wind data was obtained from ERA5 (Hersbach et al. 2020) in the absence of observational wind data.

Part of this study examined the number of tornadoes per 6-h TC track time period among the 3 phases. Only timesteps where the downshear portion of the TC was over land were considered since this is the sector of TCs where >92% of tornadoes occur (Schenkel et al. 2020). To designate these timesteps, first the downshear portion of the TC was determined by calculating the VWS vector. The outer extent of the downshear portion was demarcated by the radius from the TC center at which azimuthal-mean azimuthal wind at 925-hPa had reached 6-m s^{-1}, computed from ERA5 data following prior work (Paredes et al. 2021). A 6-m s^{-1} threshold was used since reanalyses are able to best represent the TC wind field at these weak wind speeds (Schenkel et al. 2017; Bian et al. 2021). Coastline data taken from the Global Self-consistent, Hierarchal, High-resolution Geography (GSHHG) Database at a horizontal grid spacing of ∼1 km (Wessel and Smith 1996) was used to check overlap of the downshear portion of the TC and the continental United States.

2.5 Radiosonde Data

In this study, radiosondes were taken from two sources to calculate environmental parameters such as CAPE, CIN, and SRH as well as create composite median skew T–log$P$ diagrams and composite median hodographs. Most radiosondes were from the National Oceanographic and Atmospheric Administration Integrated Global Radiosonde Archive (IGRA), version 2 (Durre et al. 2006). The IGRA has its own quality controls for physical and internal consistency for each radiosonde. The rest of the radiosondes were taken from the National Severe Storms Laboratory (NSSL)-sponsored sampling of recent landfalling TCs (Fernández-Cabán et al. 2019). For these radiosondes, the National Center for Atmospheric Research (NCAR) Atmospheric Sounding Processing Environment (ASPEN) software was utilized for processing the radiosondes and the soundings are manually verified for consistency (Wang et al. 2015; Stern et al. 2016). In addition to these checks, if wind, temperature, or moisture data are

completely missing either within 200-m of the surface or over a layer $\geq$ 1-km below a height of 8-km then the sonde was excluded (Molinari and Vollaro 2008; Schenkel et al. 2020). Only sondes that were launched between 75-km and 750-km from the center are considered in order to: 1) avoid sondes that were strongly advected by the inner-core TC winds and 2) to make sure the radius of most frequent tornado occurrence was included while not sampling environments too far from the center (Molinari and Vollaro 2010; Schultz and Cecil 2009). It is important to note that these sondes are not tornado-proximity soundings, rather, they provide a general idea of what the environment was like within a TC that transitioned and produced tornadoes.

The radiosondes that passed those qualifications were then filtered to only include those which were launched in the 49 TCs in this study and sorted into the 3 phases of extratropical transition (Table 2.5). The location of these radiosondes is shown in Figure 2.1. Note the preferential sampling of the outer core.

Phase of TC	No. of Tornadoes	No. of Radiosondes
Tropical	463	2147
Transition	373	626
Extratropical	138	622
Total	974	3395

Table 2.1: Number of tornadoes and radiosondes sorted by transition phase in this study.

The radiosondes were used to calculate environmental parameters such as 0–3-km convective available potential energy (CAPE), convective inhibition (CIN), and 0–3-km storm-relative helicity (SRH; convective cell-relative rather than TC-relative). Supercells in TCs tend to be shallow, leading to the selection of only parameters from the lower troposphere for analysis (McCaul and Weisman 1996; Schenkel et al. 2020). Composite median skew T–log$P$ diagrams and hodographs were created to compare vertical profiles between different phases of the TC. When creating profiles

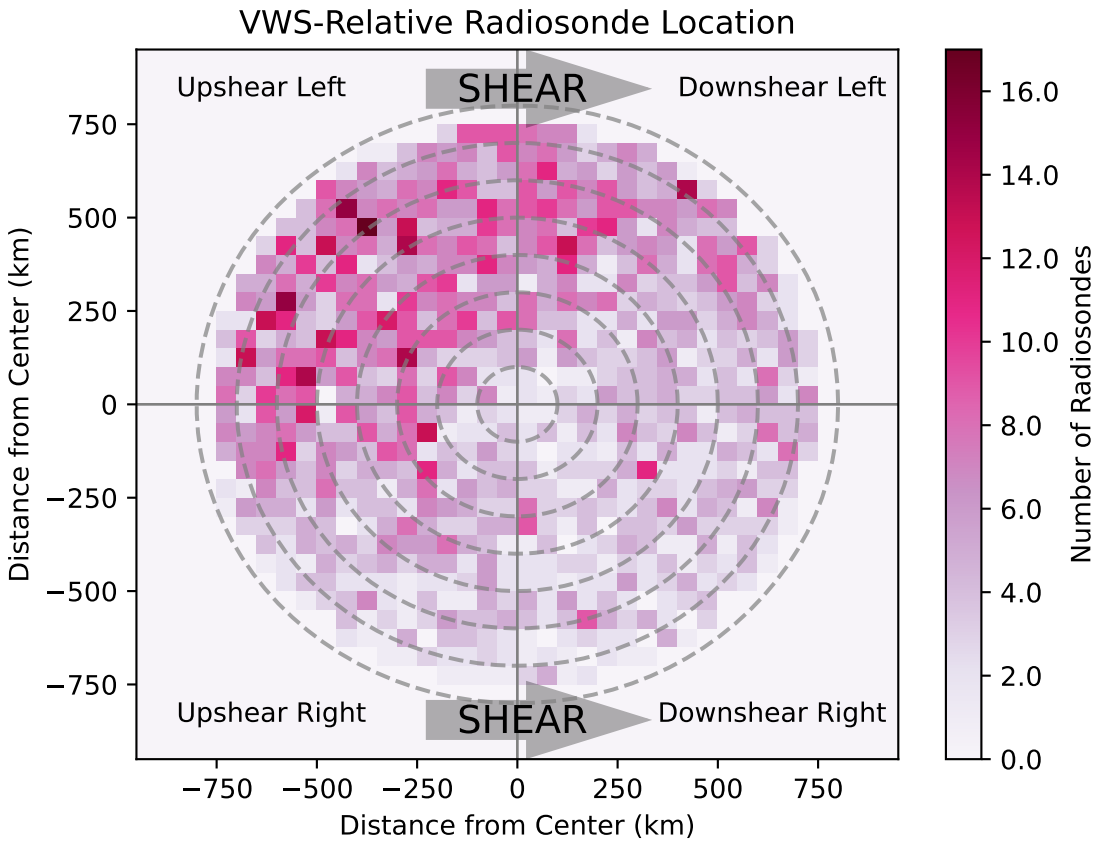


Figure 2.1: Heat map showing radiosonde location plotted in VWS-relative coordinates and with respect to the TC center.

to calculate CAPE and CIN, a mixed layer of 200-m was used as suggested for TCs in previous studies (Romps and Kuang 2011; Molinari et al. 2012). SRH was calculated using the following equation (Davies 1990):

$$SRH = \int_0^h [(\mathbf{v} - \mathbf{c}) \cdot (\mathbf{k} \times \mathbf{v}z)]\, dz \tag{2.3}$$

where $\mathbf{v}$ is the wind vector, $\mathbf{c}$ is the convective cell motion vector, and h is the layer depth. The convective cell motion vector was calculated by using methods described in Bunkers et al. (2014). The combination of these methods computes the convective cell motion vector using pressure-weighted mean winds, the Effective Inflow Base height as the base, and 65% of the most unstable parcel equilibrium level as the steering layer top (Bunkers et al. 2014).

Each sonde was also transformed into a vertical coordinate that accounts for differences in surface elevation of radiosonde launch points (Gal-Chen and Somerville 1975; Parker 2014):

$$z^* = H\frac{z - z_{sfc}}{H - z_{sfc}} \tag{2.4}$$

where H is the height of the tropopause which is assumed to be 16-km, the approximate tropopause height of Atlantic hurricanes (Duran and Molinari 2016; Gilford et al. 2017). z_{sfc} is the altitude at which the sounding was launched. The new vertical coordinate used a grid spacing of ∼50-m. The height-based vertical coordinate was used to remove any influence of terrain on synoptic and mesoscale pressure fluctuations (Parker 2014).

Radiosonde data was used to create composite hodographs that were plotted in TC-relative radial and tangential coordinates, and then organized by VWS-relative quadrant. Wind data from the radiosondes was given in zonal and meridional components and then converted to radial and tangential coordinates before the composite was taken. This conversion was done in order to account for the fact that radiosondes, while being sorted into the same VWS-relative quadrant, were released in different north-relative quadrants of the TC that could cause cancellation among the zonal and meridional components when a composite was taken due to variation in the cyclonic curvature of the flow with TC-relative azimuth.

2.6 Statistical Testing

Statistical testing was utilized to objectively determine differences among distribution statistics for each phase. Each TC tornado and radiosonde were considered to be independent of each other when performing statistical testing. For brevity purposes, when results are called "statistically different" this means that a 5000-sample

bootstrap resampling approach with replacement using two-tailed testing at the 95% confidence interval was used.

Chapter 3

Tornado and TC Characteristics

This section answers the first two questions posed in the introduction: 1) whether tornado characteristics change and 2) whether TC characteristics change in a way that could influence tornado production before, during, and after extratropical transition. This section examines tornado location, timing, damage rating, and frequency as well as characteristics of the TC and its synoptic-scale environment.

3.1 Tornado Location

To begin, TC tornado location in the United States for each of the three phases of extratropical transition is shown in Figure 3.1. All three phases as a collective have tornadoes mostly near the coast, spanning from Texas to the Mid-Atlantic, which is consistent with prior TC tornado climatologies that did not consider transition (Gentry 1983; Edwards 2012). Comparing results across the three phases shows that tornadoes become less confined to the coast and tend to occur farther north and east as the associated TC undergoes transition. This is illustrated by the extratropical phase having an average latitude that is 3.6° farther north and average longitude 3.0° farther east than the tropical phase. Tornadoes in the tropical phase, shown in Figure 3.1a, mostly occur in the southern U.S. along the Atlantic and Gulf coast. Throughout transition (Figure 3.1b), tornado location has the greatest spread, spanning from Texas to Massachusetts. Upon completion of transition (Figure 3.1c), tornadoes are confined to the Mid-Atlantic and northern Southeast. The occurrence of tornadoes farther northeastward as transition progresses supports findings from Hart and Evans

(2001) and Bieli et al. (2019), which determined that TCs tend to affect areas farther east and north in the United States during their extratropical phase than during their tropical phase.

The next two figures analyze how the TC-relative location of tornadoes changes through extratropical transition. Figure 3.2 shows a heat map of TC-relative tornado location across the three phases using a North-relative azimuthal coordinate. When comparing across the three phases, results show that the process of extratropical transition causes tornadoes to occur farther south. Tropical and transition tornadoes, shown in Figures 3.2a and b, occur in similar TC-relative positions that resemble broader TC tornado climatology, with most tornadoes occurring in the northeast quadrant within 500-km of the TC center (McCaul 1991; Schultz and Cecil 2009; Edwards 2012). Tornadoes also occur at similar TC-relative azimuths as transition begins, with tropical phase tornadoes having a median tornado location azimuth of 28° counterclockwise from east compared to 26° during the transition phase. However, the median tornado distance from the TC center increases from 305 km in the tropical phase to 345 km in the transition phase. Following the completion of transition, tornadoes occur farther south compared to the prior two phases, as suggested by a median tornado location azimuth of 1° clockwise of east (Figure 3.2c). While the extratropical phase tornadoes do not align with the location of those in Hill et al. (1966), the trend of tornadoes progressing south as transition occurs is consistent.

Since VWS has previously been proven to strongly influence tornado location (Schenkel et al. 2020, 2021), Figure 3.3 shows the TC-relative location of tornadoes relative to the direction of the VWS vector. In all three phases, tornadoes occur increasingly downshear right with increasing distance from the TC center, consistent with prior work (Schenkel et al. 2020, 2021). Furthermore, extratropical transition causes tornadoes to be more likely to occur in the downshear right quadrant. In the tropical phase, 51% of tornadoes occur in the downshear right quadrant, with 64%

and 77% for transition and extratropical phases, respectively. Tropical and transition phase tornadoes at inner TC radii occur primarily downshear left and occur more downshear right with increasing distance from the TC. In contrast, the extratropical phase begins directly downshear of the TC and ends primarily in the downshear right quadrant. This implies the importance of VWS in impacting the location of tornadoes during transition, suggested in prior work (Quinting and Jones 2016; Evans et al. 2017).

Together, these results suggest that extratropical transition is associated with tornadoes that occur farther to the north and east in the United States and a shift farther south of the TC-relative tornado location in a north-relative coordinate. The latter result may be due to a change in the VWS vector direction given that tornadoes remain in the downshear quadrants before, during, and after transition. Changes in TC-relative tornado location associated with concurrent changes in direction of VWS supports the idea that VWS is important as suggested in prior studies (Schenkel et al. 2020, 2021). Furthermore, the prominence of tornadoes in the downshear right quadrant during the extratropical phase could be due to stronger entrainment of ambient colder, more stable air to the north or left of the shear vector.

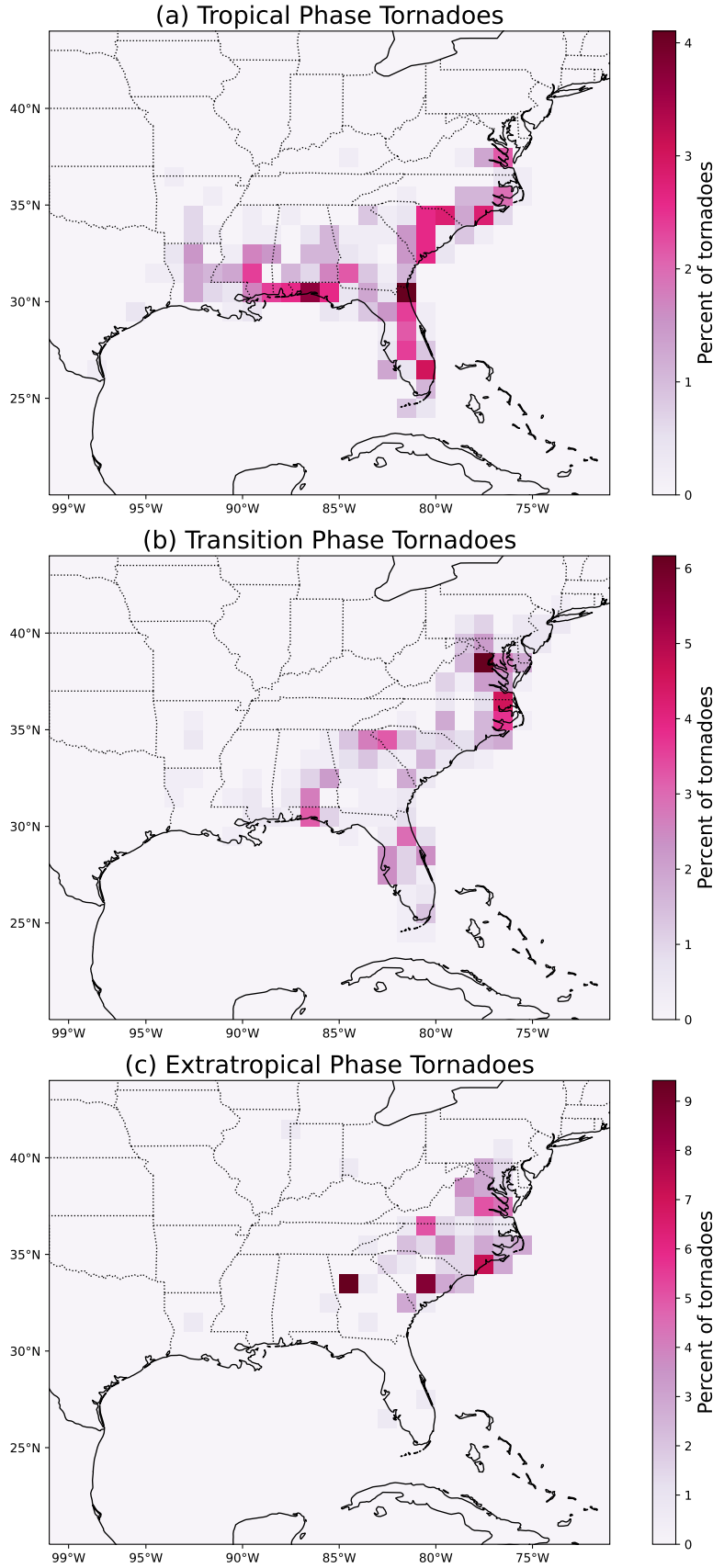


Figure 3.1: Heat map showing the location of tornado occurrence in the United States for (a) tropical, (b) transition, and (c) extratropical phase tornadoes.

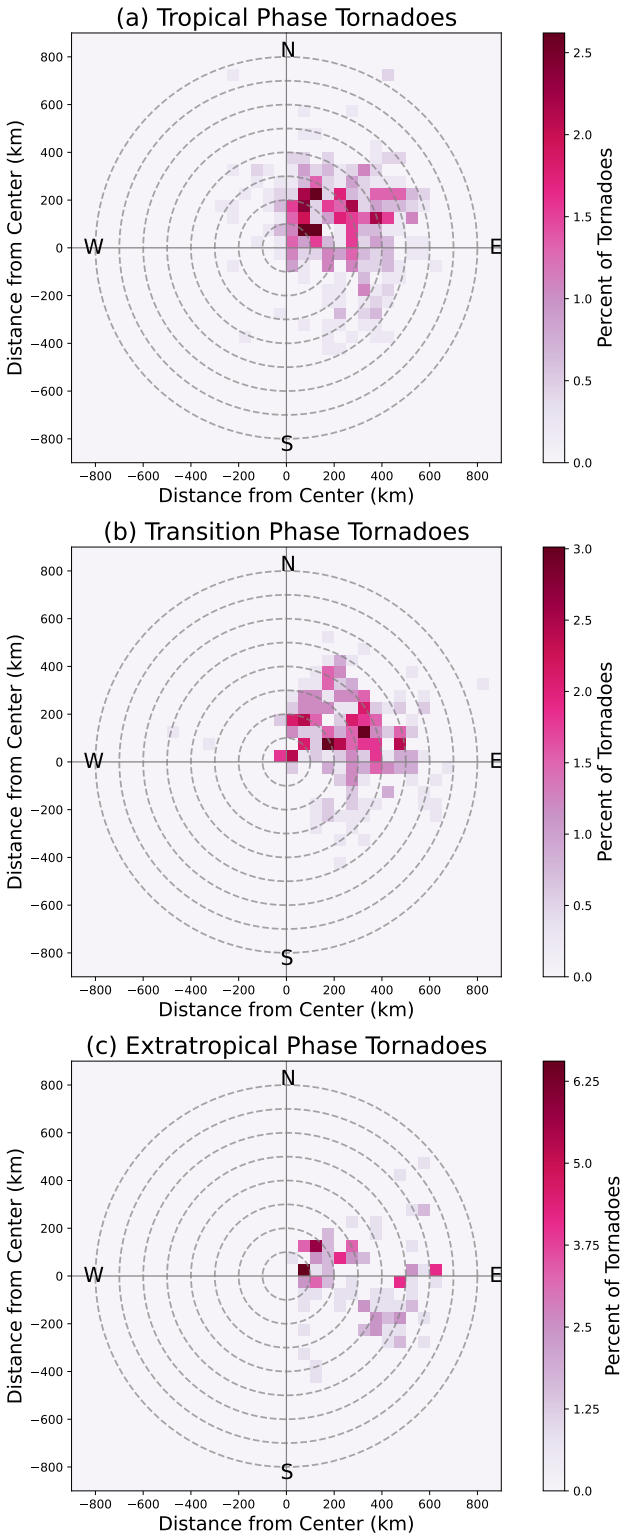


Figure 3.2: Heat map showing TC-relative tornado location plotted in North-relative coordinates and with respect to TC center for (a) tropical, (b) transition, and (c) extratropical phase tornadoes. Dashed gray lines represent range rings in 100 km intervals from the TC center.

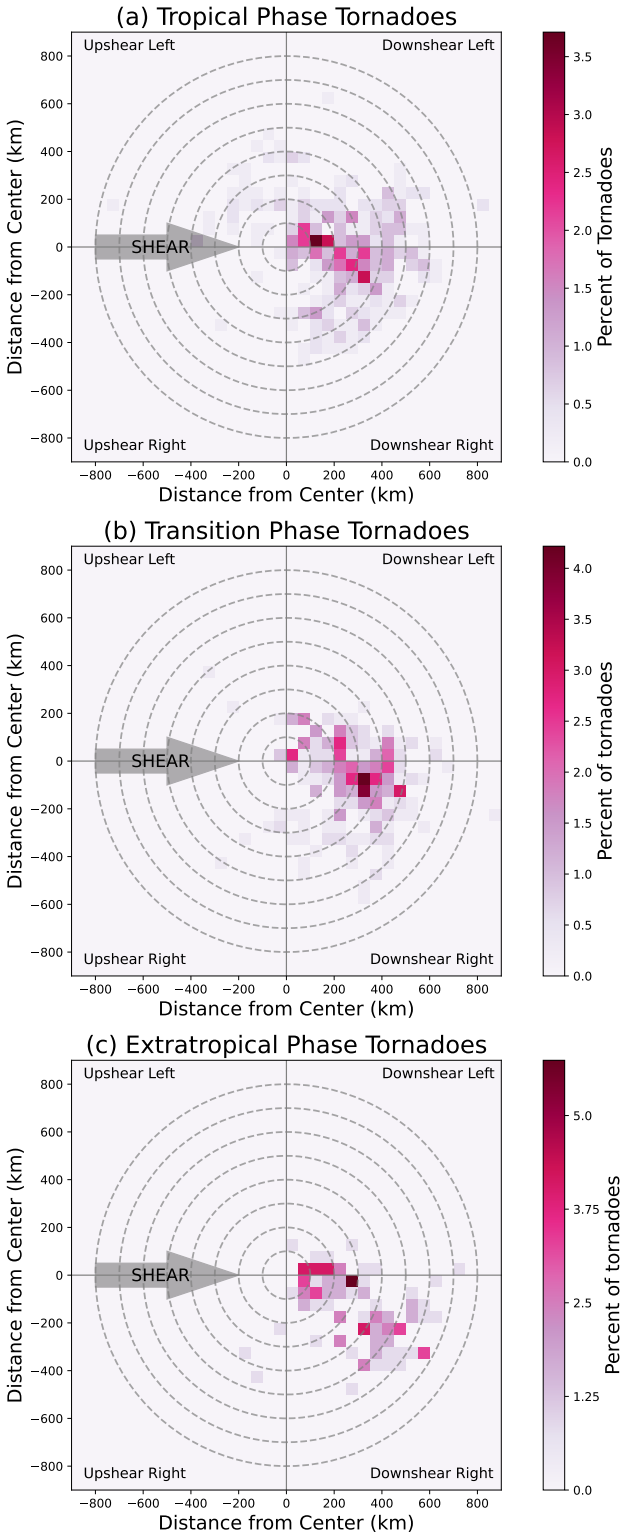


Figure 3.3: As in Figure 3.2, except plotted in VWS-relative coordinates. The VWS vector (gray arrow) has been rotated to always point to the right of the plot, with tornadoes rotated by the same angle.

3.2 Tornado Timing, Frequency, and Damage

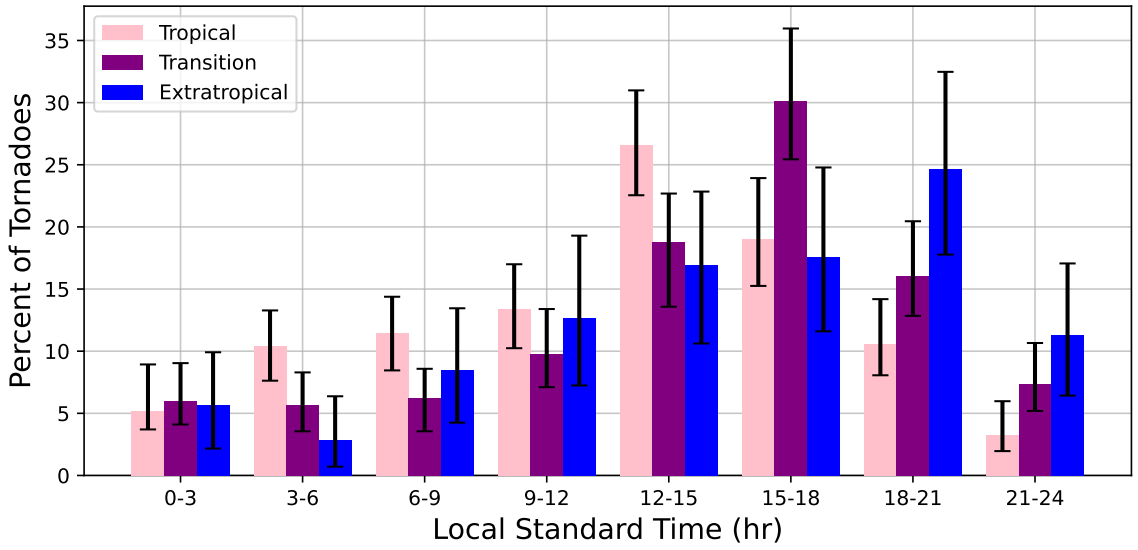


Figure 3.4: Histogram of percent of tornadoes observed binned by local standard time in the tropical phase (pink), transition phase (purple), and extratropical phase (blue). Black error bars show the 95% confidence interval computed using a 5,000 bootstrap resampling approach with replacement.

Analysis of the diurnal variability of TC tornadoes shows that as extratropical transition progresses, tornadoes are more likely to occur later in the day. Figure 3.4 shows that all three phases are associated with a strong daytime peak and a nighttime minimum in tornado occurrence, consistent with climatologies for all TC tornadoes (McCaul 1991; Schultz and Cecil 2009; Edwards 2012). Tropical phase tornadoes experience this peak in the early afternoon, with 27% occurring between 12–15 LST. In comparison, 30% of transition phase tornadoes occur between 15–18 LST, while a peak of 25% for extratropical phase tornadoes occur between 18–21 LST. Transition phase has the strongest peak and is the only phase whose peak is significantly different from the surrounding bins of the same phase. The extratropical phase has the weakest peak, around local sunset, which resembles that for non-TC tornado climatology and could indicate that convective-scale environments are similar between these two modes (Schultz and Cecil 2009). Extratropical phase tornadoes

during their peak and the following three hours have a significantly greater portion of tornadoes than the tropical phase in each 3-h bin.

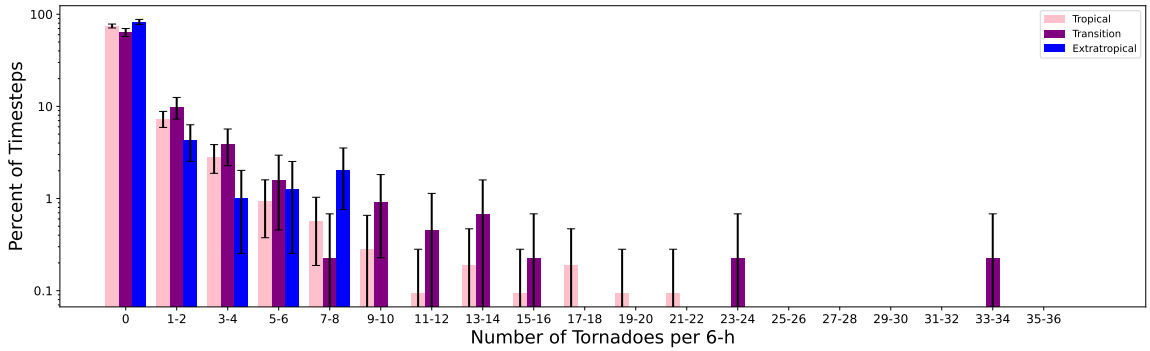


Figure 3.5: As in Figure 3.4, except showing number of tornadoes per 6-h with the y-axis using a logarithmic scale. Only periods when the TC was over land were considered. 6-h temporal resolution shown due to Best-Track TC dataset having this resolution.

Frequency of tornado occurrence per 6-h was investigated and is shown in Fig. 3.5. The life cycle of each TC was divided into 6-h segments (timesteps), matching the Best-Track TC track reporting interval as well as the interval used in prior work (Schenkel et al. 2020, 2021). Moreover, prior work has also used a 6-h timestep given the variability in the structure of the TC and its synoptic-scale environment over the TC track (Rios-Berrios et al. 2016a,b). For each 6-h timestep, the number of tornadoes is totaled within ±3 h. Only those 6-h periods in which the downshear sector of the TC overlapped with the continental United States are considered, since this is the region where tornadoes are most common (Schenkel et al. 2020; Paredes et al. 2021). Figure 3.5 shows that TCs do not spawn tornadoes for most 6-h time periods in all three phases. Specifically, 75%, 63%, and 81% of 6-h times in the tropical, transition, and extratropical phases are not associated with tornadoes. The percentage of 6-h times with 0 tornadoes in the extratropical phase is significantly higher than in the transition phase. When only considering timesteps with $\geq$1 tornado, the median number of tornadoes is 2 for the tropical and transition phases and 2.5 for the extratropical phase, suggesting small differences in the number of tornadoes

typically spawned among phases. However, differences do exist for 6-h times with enhanced numbers of tornadoes. In particular, the extratropical phase is characterized by a narrower distribution with statistically similar percentages, especially from 3–8 tornadoes per 6-h, and no 6-h times exceeding ≥10 tornadoes per 6-h. For comparison, 2% of tropical phase timesteps and 5% of transition phase timesteps have ≥10 tornadoes per 6-h.

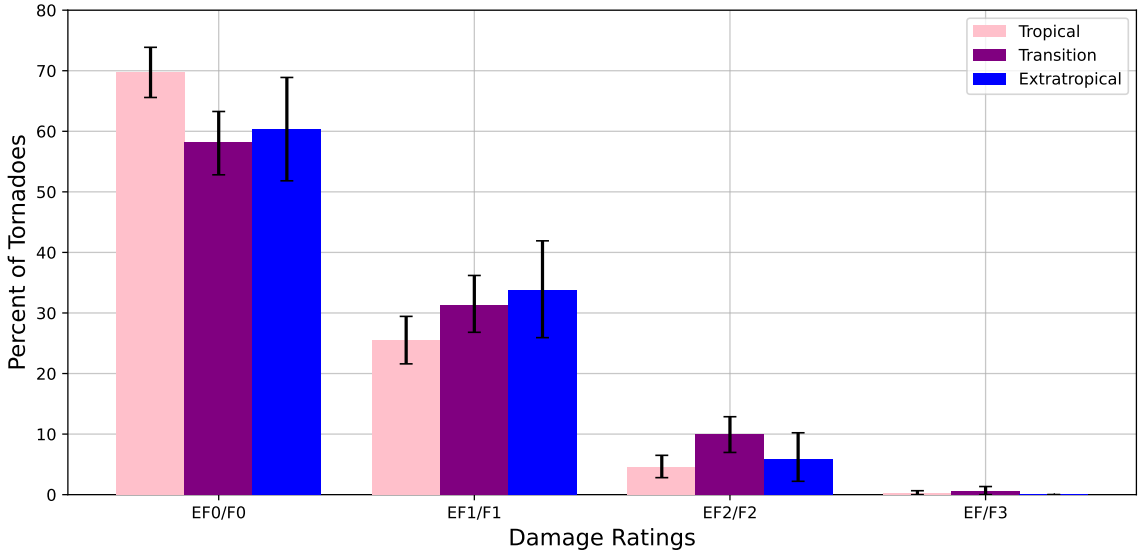


Figure 3.6: As in Figure 3.4, except showing tornado damage ratings.

Extratropical transition is also associated with differences in the damage rating of TC tornadoes. Figure 3.6 shows that most TC tornadoes in all phases have damage ratings in the EF0/F0 or EF1/F1 categories with no cases classified with damage ratings exceeding EF3/F3, consistent with prior work (Edwards 2012; Edwards and Mosier 2022). As transition begins, the likelihood of more damaging tornadoes increases, as indicated by the significant difference in EF0/F0 and EF2/F2+ tornadoes between the tropical and transition phases. In particular, 70% of tropical phase tornadoes are associated with an EF0/F0 rating, which is greater than the extratropical phase (60%) and statistically greater than the transition phase (58%). While the transition phase has the lowest number of EF0/F0 tornadoes, it has the highest percent of more damaging tornadoes (≥EF2/F2) at just over 10%, which is statistically

different from the tropical phase at 5%. This figure also shows that after transition has begun, the chances of damaging tornadoes remains mostly the same since the transition and extratropical phases are never significantly different from each other.

In this subsection, extratropical transition was found to impact the timing, frequency, and damage rating of tornadoes. Tornadoes occur later in the day time as transition progresses, indicating that the processes associated with the diurnal cycles may be different. The early afternoon peak for the tropical phase could be associated with a TC diurnal cycle identified in Dunion et al. (2014), in which cloud-top cooling and sometimes an accompanying TC rainband propagate away from the TC center and reach outer radii by early afternoon (Ditchek et al. 2019, 2020). The process and completion of transition yields fewer tornadoes that are associated with more damage than prior to transition. Schenkel et al. (2021) found that inland TC environments are associated with stronger VWS and reduced CAPE, which could explain this discrepancy between frequency and damage ratings. Overall, these disparities in diurnal variability, frequency, and damage ratings suggest that there may be differing processes that influence tornado production before, during, and after extratropical transition.

3.3 Characteristics of the TC and Its Synoptic-Scale Environment

Figure 3.7 shows the distribution of TC maximum 10-m sustained wind speed (i.e., TC intensity) at the time of tornado occurrence. As transition progresses, tornadoes are more likely to occur in TCs with weaker intensities, confirmed by comparing the median TC intensity values between the tropical (53-kt), transition (46-kt), and extratropical phases (25-kt). TC intensities during the tropical and transition phases have broad distributions that are skewed toward stronger intensities with adjacent

bars lacking significant difference. The tropical phase has the greatest spread with tornadoes that occur at intensities between 15–150-kt. 30% of tornadoes during the tropical phase occurred when the TC was at tropical storm strength (between 34–63-kt). The extratropical phase has the narrowest distribution and sharpest peak with all tornadoes occurring at TC intensities of 15–50-kt and 73% of tornadoes between just 20 and 40-kts. The decrease in TC intensity associated with tornadoes throughout extratropical transition is consistent with the typical weakening of TCs following transition start (Hart and Evans 2001; Evans and Hart 2008).

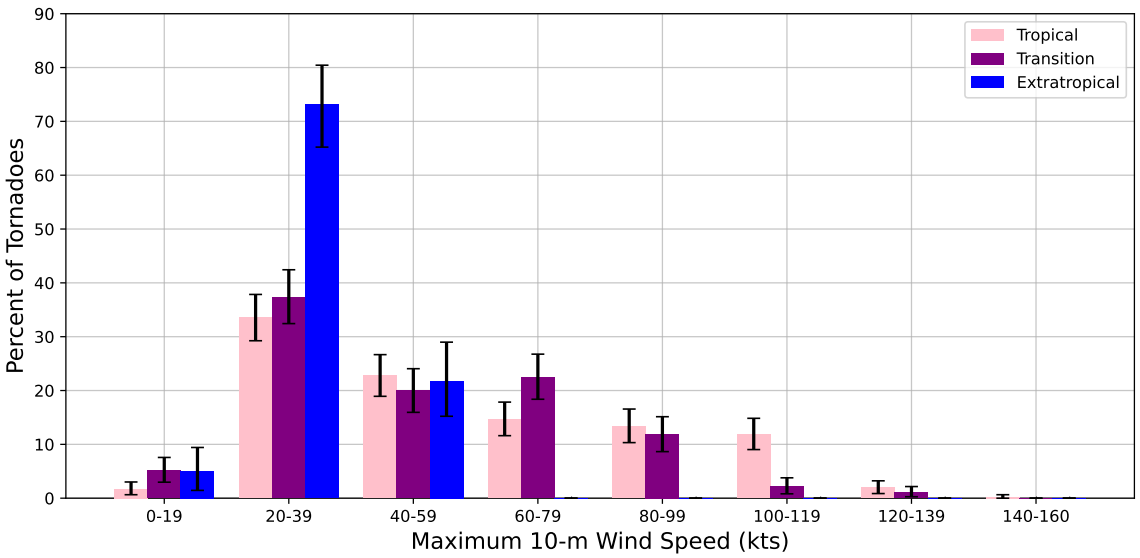


Figure 3.7: As in Figure 3.4, except showing TC intensity as the Best-Track maximum 10-m wind speed (kt) interpolated to the time of tornado occurrence.

The outer wind field size of transitioning TCs that spawn tornadoes varies before, during, and after extratropical transition. This is shown in Figure 3.8, which compares the distributions of radii at which the azimuthal-mean 925-hPa azimuthal wind of the TC equals 6-m s^{-1} (r_6) derived from reanalysis data. This metric has been previously used to study the relationship between TC outer size and tornadoes (Paredes et al. 2021). The median size of the TC at the time of tornado occurrence in the transition phase (816-km) is largest, followed by the tropical (702-km) and extratropical phases (635-km). This expansion of the wind field during transition implied in these results is

consistent with prior work (Hart et al. 2006; Evans and Hart 2008). The tropical and transition phases have clear peaks of 48% and 42%, respectively, and are significantly different from surrounding bins of respective phase. In contrast, the extratropical phase peak is weaker and not significantly different from surrounding bins given its broad distribution. Larger TC outer size during transition could explain why the median distance of tornado occurrence from the TC (shown in Figure 3.2) is greater during the transition phase than other phases, as implied in prior work (Paredes et al. 2021).

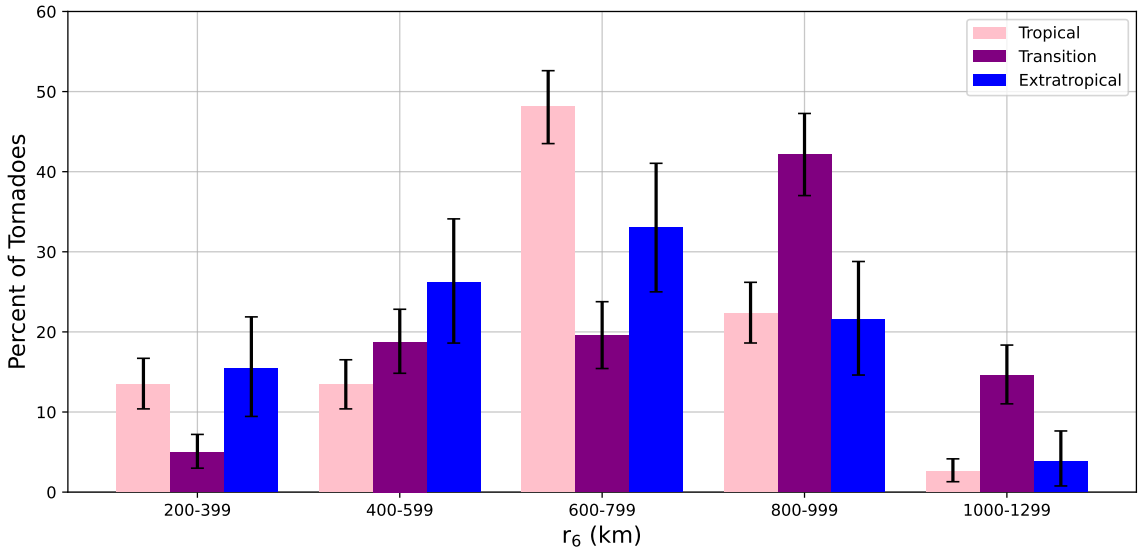


Figure 3.8: As in Figure 3.4, except showing TC near-surface outer wind field size as the radius at which the azimuthal-mean 925-hPa azimuthal wind equals 6 m s^{-1} (r_6; km), calculated from the ERA-5 reanalysis, interpolated to the time of tornado occurrence.

The remaining plots focus on examining differences in the synoptic-scale environment of the TC by examining how tornado occurrence varies with different magnitudes and directions of VWS (i.e., synoptic-scale, 850–200-hPa vertical wind shear) that impact the TC. Figure 3.9 shows that as transition progresses, tornadoes occur in stronger and more variable magnitudes of VWS. This increase in VWS during and after transition is consistent with an increase in baroclinicity that is suggested in current conceptual models of extratropical transition (Klein et al. 2000; Evans et al.

2017). In addition to having the strongest shear, the extratropical phase has the broadest distribution, spanning from ∼8–30 m s^{-1} and with most adjacent bins lacking statistical difference. In contrast, the transition phase has a similar range albeit shifted towards weaker values, with most adjacent bins being statistically different from one another. The tropical phase has a clear peak in the weaker magnitudes of VWS centered near 10 m s^{-1}, as expected given TCs typically exist in low-to-moderate VWS (Rios-Berrios and Torn 2017). Previous work has defined "strong" VWS as ≥∼11 m s^{-1}, which more strongly concentrates tornadoes downshear and creates more favorable environments for more tornadoes to occur (Schenkel et al. 2020, 2021). During the tropical phase, only 30% of tornadoes occurred in "strong" shear, whereas the transition and extratropical phase had 86% and 89% of their tornadoes occurring in "strong" shear. The predominance of stronger VWS in the transition and extratropical phases is consistent with a larger percentage of tornadoes in the downshear quadrant compared to the tropical phase, shown in Figure 3.3.

While VWS magnitude becomes more variable as TCs transition, Figure 3.10 shows that the opposite is true for VWS direction. The majority of tornadoes in all three phases occur when the VWS is southwesterly. This prominence of southwesterly shear across all phases is also similar to prior work (Corbosiero and Molinari 2003; Schenkel et al. 2020). Tropical phase tornadoes can occur when the VWS is out of almost all directions, only lacking tornadoes when VWS is northeasterly. However, as extratropical transition progresses, a greater portion of tornadoes occur when VWS is southwesterly. All three phases have significantly different percentages of TCs with southwesterly VWS from each other, 65%, 78%, and 91% for tropical, transition, and extratropical, respectively. Extratropical phase tornadoes being most likely to occur when VWS is southwesterly could be in association with the flow downstream of an approaching upstream upper-tropospheric trough (Hart et al. 2006; Sarro and Evans

2022). The westerly shift in VWS through extratropical transition may help explain the southward shift of tornado location in Figure 3.2.

In summary, the characteristics of the TC and synoptic-scale environment associated with tornado occurrence differ before, during, and after extratropical transition. Specifically, tornadoes occur in TCs with weakening intensities and larger outer sizes in the transition phase, while both intensity and outer size decreased following transition, similar to prior conceptual models of extratropical transition (Hart and Evans 2001; Jones et al. 2003; Evans and Hart 2008). VWS magnitude during tornado occurrence increases and becomes more variable through transition, while VWS direction becomes more concentrated in the southwest direction. Stronger VWS implies that there was a stronger horizontal temperature gradient that the TC was interacting with, which would increase the asymmetries in kinematic and thermodynamic structure of the cyclone. These changes in TC structure and in its synoptic-scale environment, as implied by VWS, are consistent with prior extratropical transition climatologies and case studies (Klein et al. 2000; Hart and Evans 2001; Evans and Hart 2008). The changes also may help explain differences in the location and number of tornadoes among the three phases of extratropical transition, and likely also impact convective-scale environments within the TC, which is shown in the next section.

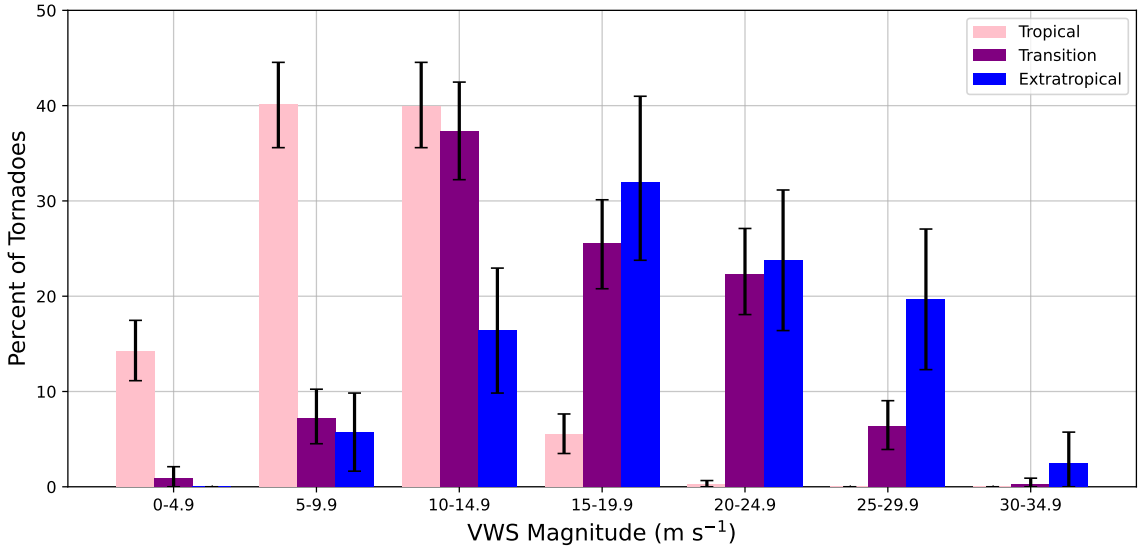


Figure 3.9: As in Figure 3.4, except showing interpolated VWS magnitude (m s^{-1}) to the time of tornado occurrence.

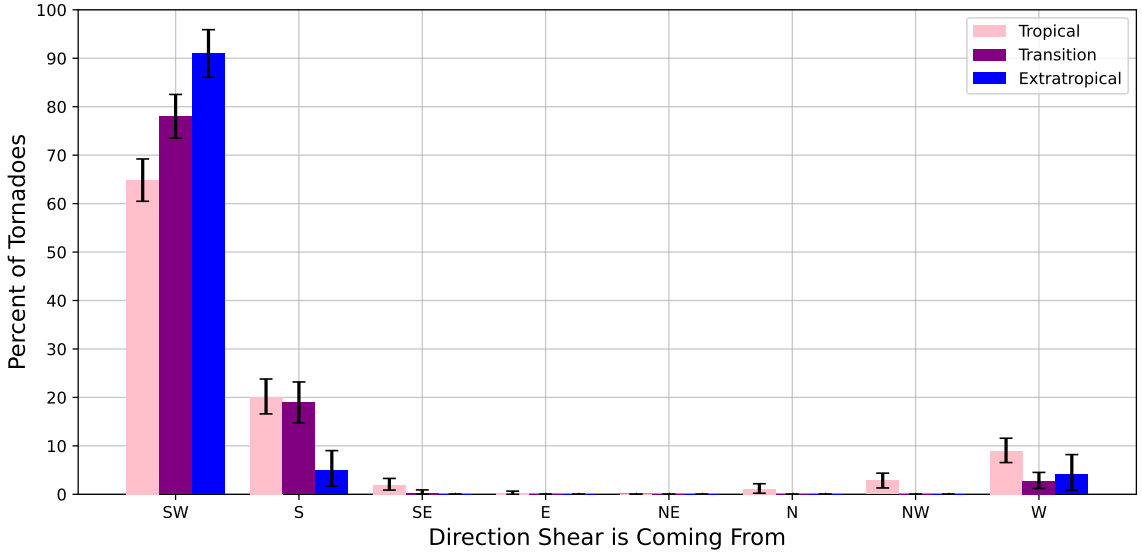


Figure 3.10: As in Figure 3.4, except showing interpolated 850–200-hPa VWS direction to the time of tornado occurrence.

Chapter 4

TC Convective-scale Environments

This section answers the third question posed in the introduction: How the convective-scale environments within a TC change through extratropical transition. The thermodynamic characteristics of the convective-scale environments through transition were examined first, followed by kinematic environmental characteristics.

4.1 Thermodynamic Characteristics

The distributions of 0–3-km CAPE and CIN in each VWS-relative quadrant of TCs for each of the three phases are shown in Figures 4.1 and 4.2, respectively. In general, as extratropical transition progresses, CAPE decreases in all quadrants although differing by quadrant in the timing and magnitude of decrease. Decreasing CAPE through transition mostly matches findings in Schenkel et al. (2021), which found that CAPE tended to decrease as TCs progressed farther inland in all quadrants except for the downshear right. The change in median magnitude of CIN is almost never significant between phases in a quadrant, yet the lower quartile shifts toward larger magnitudes. CAPE values in the downshear right quadrant and, to a lesser extent, the remaining three quadrants in the tropical phase are consistent with ranges favorable for TC tornado production ($\sim$100–200 J kg^{-1}; Baker et al. 2009; Eastin and Link 2009). Most CIN values in all quadrants and phases are within known CIN ranges for TCs that produce tornadoes ($\sim$–20–0 J kg^{-1}; Baker et al. 2009; Molinari et al. 2012). In the tropical phase, CAPE is greatest (with a median of 138 J kg^{-1}) and the magnitude of CIN is smallest (median of –8 J kg^{-1}) in the downshear right quadrant

compared to the others. Through transition the downshear right quadrant continues to have the most favorable values of CAPE and CIN for tornado production, with increasingly distinguishes itself from other quadrants. The extratropical phase has the lowest values of CAPE in all quadrants and increased range in magnitude of CIN, suggesting it to be less favorable for tornado production. This could be one reason why the number and frequency of tornadoes are reduced in the extratropical phase, as shown in Table 2.5 and Figure 3.5. However, even in the extratropical phase, the upper quartile of the downshear right CAPE remains within the favorable range for tornadoes.

Further insight into the impact of the increasingly baroclinic environment on convective-scale environments within the TC is gained when comparing CAPE and CIN across quadrants through transition. Both of the left-of-shear quadrants experience a significant decrease in CAPE between the tropical and transition phases (showing decreases of 91-J $kg^{-1}K^{-1}$ and 56-J kg^{-1} in median values, respectively), while the right-of-shear quadrants show no significant changes in median values (3-J kg^{-1} and 6-J kg^{-1}, respectively). The left-of-shear quadrants also are associated with shifts in the lower quartile towards greater magnitudes of CIN between the tropical and transition phase that are greater than that of the right-of-shear quadrants. Assuming thermal wind balance between the VWS vector impacting the TC and the associated horizontal temperature gradient, these results could reflect the presence of a colder, more stable environment to the left of the VWS vector as transition begins. This would make sense, as the left-of-shear quadrants are often to the north of the TC given the typical westerly component to the VWS (Figure 3.10). Strong decreases in CAPE and increased ranges of CIN only occur at the end of transition for the quadrants to the right of the VWS vector, further into transition than the left-of-shear quadrants. Specifically, both right-of-shear quadrants are characterized by significant changes in median CAPE values (105-J kg^{-1} downshear right and 66-J kg^{-1} upshear right) between the transition and extratropical phases.

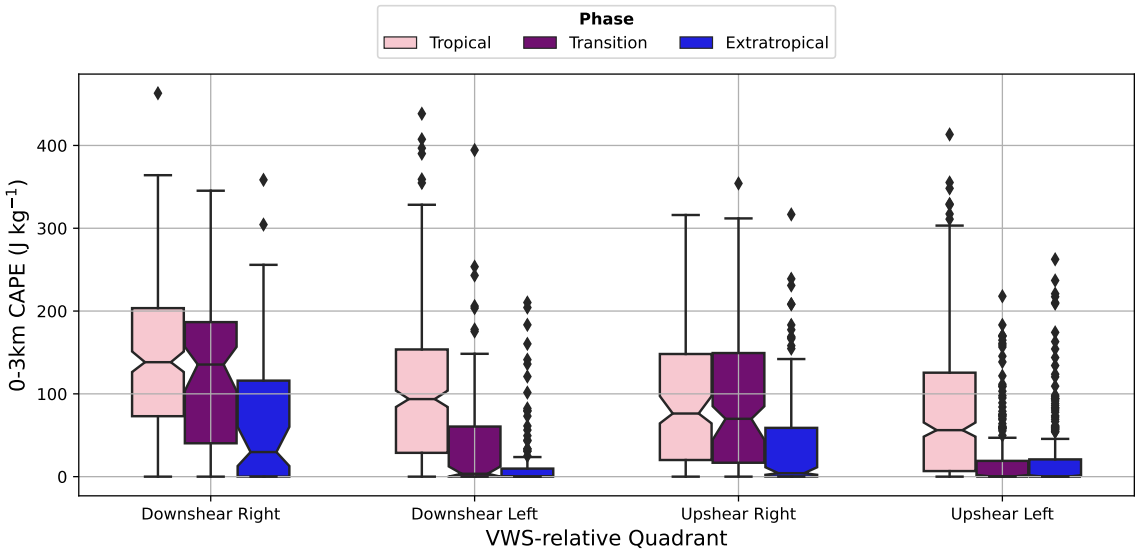


Figure 4.1: Box-and-whiskers plots of 0–3-km CAPE (J kg^{-1}) values across phases and VWS-relative quadrants. The box perimeter shows the interquartile range. The line across the middle indicates the median, while the notches represent the 95% confidence interval of the median. Whiskers extend from both the bottom of the box (25th percentile) to the lowest observed datum and from the top of the box (75th percentile) to 1.5x the interquartile range. Diamonds indicate outliers.

Composite median skew T–log$P$ diagrams created for each phase and quadrant show the vertical structure of the temperature and moisture changes throughout extratropical transition (Figure 4.3). As transition progresses, all quadrants show decreases in moisture and temperature, especially in the lower troposphere. The right-of-shear quadrants show modest changes in dewpoint and temperature profiles between the tropical and transition phases. Consistent with the timing of significant decreases in CAPE and CIN, these quadrants become cooler near the surface and drier throughout most of the troposphere following transition. The downshear right quadrant, shown in Figure 4.3d, is characterized by the smallest decrease in median surface temperatures (∼3°C) before and after transition. Contrary to the the rest of the troposphere, the near surface relative humidity in the upshear right quadrant (Figure 4.3c) increases into the extratropical phase, as the median dewpoint only decreases by about ∼2°C whereas the median temperature decreases by about ∼5°C. The left-of-shear quadrants (Figures 4.3a and b) typically show substantial cooling

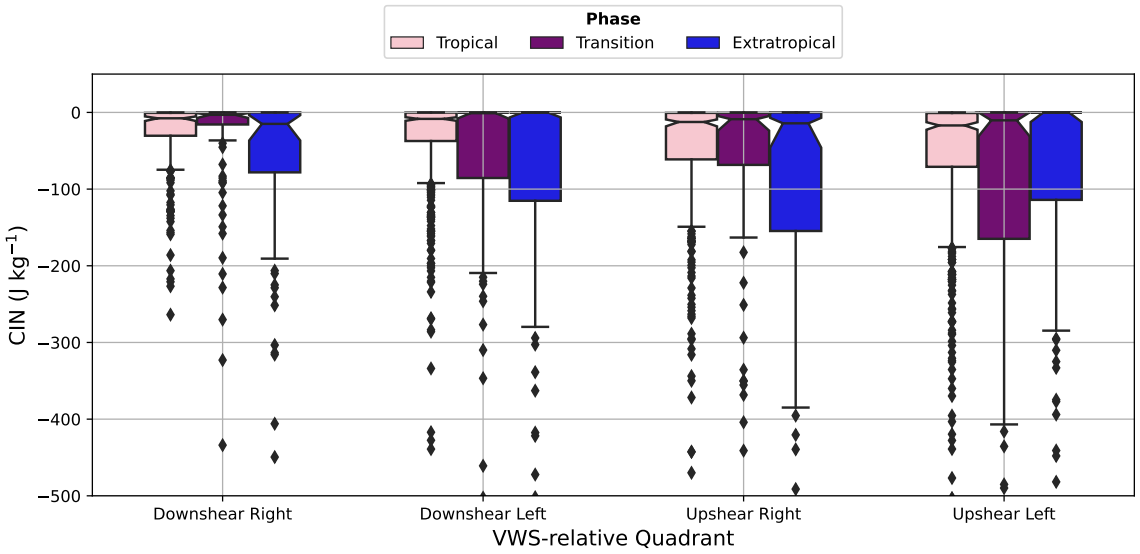


Figure 4.2: As in Figure 4.1, except for CIN (J kg^{-1}) up to 500-hPa. Some outliers are excluded from this figure to more clearly highlight the middle of the distribution.

and drying between the tropical and transition phases, again suggesting the more rapid interaction of these quadrants with cooler, drier air. Additional cooling and drying occurs following transition, resulting in overall near-surface temperature decreases of ∼7°C between the tropical and extratropical phases. However, the upshear left quadrant cools and dries out much more in the lower troposphere and peaks in the middle troposphere. The particularly dry middle and upper troposphere in the upshear left quadrant and, to a lesser extent, the upshear right quadrant may be associated with: 1) VWS-induced injection of dry air into the TC circulation (i.e., "ventilation") and 2) vertical tilting of the TC downshear which induces subsidence upshear (Jones 1995; Tang and Emanuel 2010).

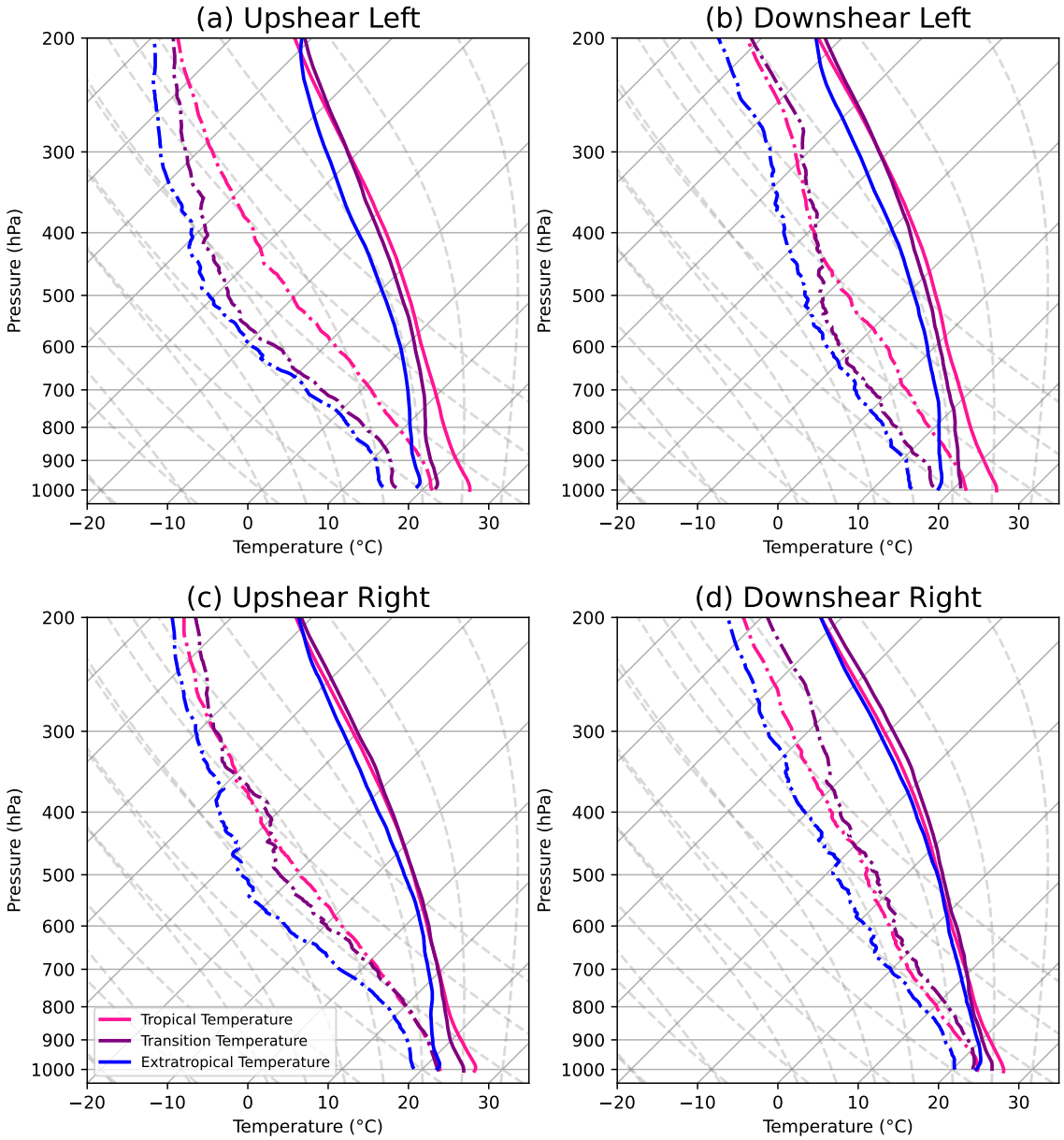


Figure 4.3: Composite median skew T–log$P$ diagrams for the (a) upshear left, (b) upshear right, (c) downshear left, and (d) downshear right quadrants in the tropical (dark pink), transition (purple), and extratropical (blue) phases. Temperature is illustrated by the solid lines and dashdot lines represent dewpoint.

4.2 Kinematic Characteristics

The kinematic characteristics of each quadrant and phase are first examined using 0–3-km SRH. Figure 4.4 shows how SRH responds to extratropical transition in each of the quadrants. The values of SRH across all phases and quadrants are small compared to non-TC environments, with only the downshear right quadrant having values consistent with known ranges associated with TC tornadoes (100–260-m^2s^{-2}; McCaul and Weisman 1996; McCaul et al. 2004). As transition progresses, median SRH shows no significant changes among the left-of-shear quadrants in each phase, although the upper quartile shifts towards larger magnitudes. This result is broadly consistent with Schenkel et al. (2021), which showed no significant changes in SRH in these quadrants as TCs move inland regardless of phase. In contrast, the right-of-shear quadrants are associated with a shift in entire distributions towards stronger helicity values at the beginning of transition Specifically, median values of SRH between the tropical and transition phases within the downshear right (58-m^2s^{-2} to 184-m^2s^{-2}) and upshear right quadrants (24-m^2s^{-2} to 58-m^2s^{-2}) show significant increases in magnitudes of SRH. Thereafter, there are no significant changes in helicity between the transition and extratropical phase in the upshear right quadrant and a non-significant yet notable decrease in the downshear right quadrant. Schenkel et al. (2020) found that SRH in the downshear right quadrant tended to increase in TCs with greater VWS, and hence, the increase in VWS at the beginning of transition shown in Figure 3.9 may explain the simultaneous increase in helicity. This significant increase in SRH between the tropical and transition phases in the downshear right quadrant could explain why the transition and extratropical phases have a higher proportion of damaging tornadoes (Figure 3.6).

Figure 4.5 shows composite median hodographs for each quadrant throughout extratropical transition using TC-relative tangential and radial winds, similar to prior TC tornado studies (McCaul 1991; Baker et al. 2009). TC motion was removed from

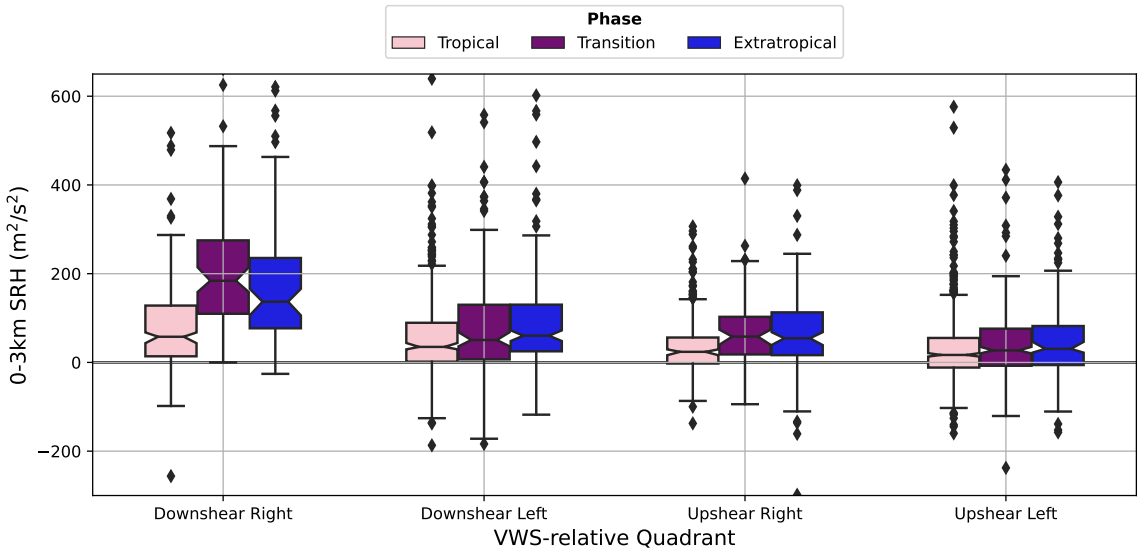


Figure 4.4: As in Figure 4.1, but for 0–3-km SRH (m^2 s^{-2}). Note that whiskers in this figure extend from the box edges to 1.5x the interquartile range in both directions.

each vertical level in an effort to remove ambient winds from the hodographs (McCaul 1991; Baker et al. 2009). However, this assumes a horizontally and vertically-uniform ambient flow, which is not always realistic during and after extratropical transition in a strongly baroclinic environment (Thorncroft et al. 1993). These plots depict changes in the vertical structure of the TC winds associated with the helicity changes shown in Figure 4.4. In all quadrants, the TC radial and tangential winds strengthen from the tropical to transition phases and, excluding the upshear right quadrant, weaken in the extratropical phase. This strengthening of the tangential component of the TC winds is particularly evident in the downshear right quadrant in the boundary layer at transition onset, resulting in enhanced speed shear and veering in the vertical direction. This enhanced shear and veering at the beginning of transition is consistent with prior work (Schenkel et al. 2020, 2021) as well as with the timing of significant increases in SRH during transition shown in Figure 4.4. The downshear right quadrant has the strongest increases in both tangential and radial winds potentially due to: 1) enhancement of the TC secondary circulation associated with VWS-induced tilting of the TC, 2) stronger superposition of ambient and TC winds in this quadrant,

3) development of a lower-tropospheric jet in association with warm-conveyor belt development, or 4) the expansion of TC wind field during transition, as shown or implied in prior work (Evans and Hart 2008; Evans et al. 2017; Schenkel et al. 2020). The increasing wind magnitude between the tropical and transition phases could be explained by the preferential sampling of the outer core of the TC (Figure 2.1), whereby the wind field expands into at the beginning of transition (Figure 3.8. TC winds in the downshear right quadrant of the extratropical phase are weaker than the transition phase, particularly in the tangential component. This could be because of the typical weakening of the TC in the extratropical phase, with weakening winds and thus weakening lower-level shear (Hart and Evans 2001; Sarro and Evans 2022).

This analysis has shown that as extratropical transition progresses, the downshear right quadrant has the most favorable kinematic and thermodynamic conditions for tornado occurrence. CAPE tends to decrease whereas the range of CIN values increase through transition, with the lower troposphere becoming colder and drier as the TC embeds itself farther into baroclinic zone. SRH and the vertical structure of TC winds in the downshear right quadrant tend to become particularly strong and favorable for tornado occurrence during the transition phase, followed by weakening in the extratropical. Conditions in the other quadrants become less favorable or remain the same, similar to results shown in Schenkel et al. (2021). The potential development of a lower-tropospheric jet in association with the warm conveyor belt also asymmetrically enhances the TC winds, as well as continuing to bring warm and moist air to the downshear right quadrant to maintain CAPE. This could explain why, in Figure 3.3, tornadoes occur increasingly in the downshear right quadrant as transition progresses.

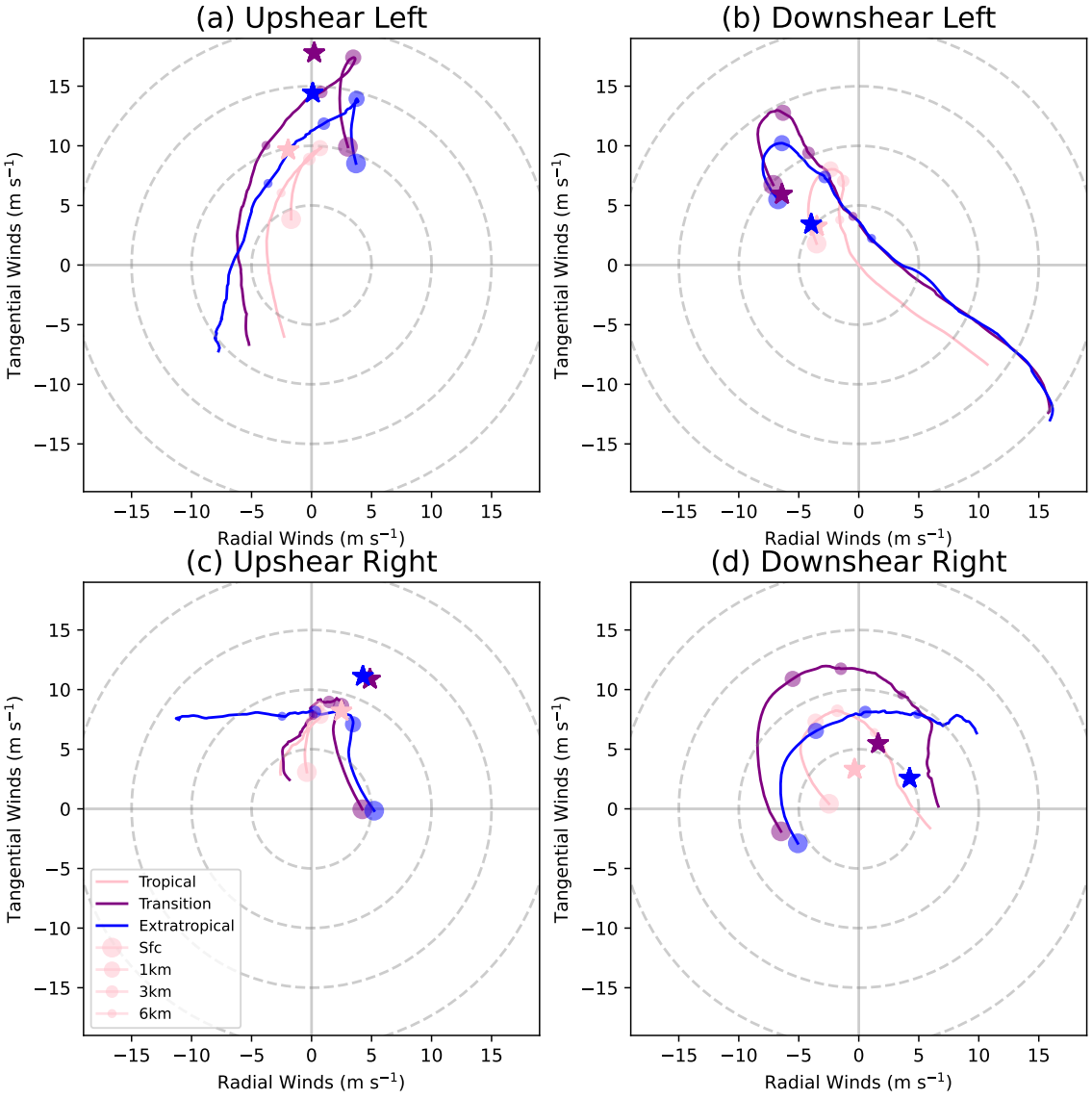


Figure 4.5: Composite median hodographs for the (a) upshear left, (b) downshear left, (c) upshear right, and (d) downshear right quadrants in the tropical, transition, and extratropical phases for transitioning TCs. TC motion has been removed from each radiosonde in an attempt to isolate changes in TC winds. Stars represent composite median Bunkers storm motion vector for each phase in each VWS-relative quadrant. Dashed rings are shown at 5-m s^{-1} intervals. Black circles of different sizes show winds at the surface (i.e., typically below 10 m), 1-km, 3-km, and 6-km heights. Note: All three phases begin with weakly cyclonic or even anticyclonic inflow winds in the downshear right quadrant, similar to previous work (Baker et al. 2009).

Chapter 5

Summary and Discussion

This study investigated how the extratropical transition of TCs impacts tornado occurrence and their associated convective-scale environmental characteristics. To accomplish this, the life cycle of each extratropically transitioning TC that spawned tornadoes was divided into three phases to examine how tornadoes, the characteristics of the associated TCs, and the environments they occur in differ. The first part of the study consisted of building a climatology comprised of tornado and TC data from 1995–2020, before, during, and after extratropical transition. The second part of the study analyzed radiosondes within extratropically transitioning TCs to analyze how convective-scale environments changed through transition in order to provide context to the climatology results.

These results showed that extratropically transitioning TCs spawned the most tornadoes during the tropical phase followed by the transition and extratropical phases. The 6-h frequencies of tornadoes were very similar before and during transition, before reducing during the extratropical phase. Tornadoes typically occur farther north and east across the United States as extratropical transition progressed, consistent with the recurvature of transitioning TCs towards poleward latitudes. An analysis of the TC-relative location of tornadoes showed a southward shift during and after extratropical transition, coincident with increasing tornado occurrence in the downshear right quadrant. Through transition, the "peak" time of tornado occurrence became later, shifting from a peak in the early afternoon to the early evening following transition. During and after transition, tornadoes were significantly more likely to be more damaging than prior to transition.

TC characteristics that impact TC tornado occurrence also changed during extratropical transition. Specifically, the extratropical phase was associated with weakening of the TC, which was coincident with an increase in VWS. The direction of VWS also became more strongly southwesterly as transition progressed. In addition to weakening, the outer size of the near-surface TC wind field initially expanded during transition, before contracting slightly thereafter.

Analysis of convective-scale environments diagnosed by radiosondes showed that as transition progressed, the downshear right quadrant was the only quadrant with a combination of kinematic and thermodynamic characteristics that was most favorable for tornadoes during all three phases of transition. In particular, this quadrant was most favorable for tornado production during transition, when CAPE had yet to decrease significantly, CIN was at its lowest magnitude, and SRH was at its largest magnitude given increases in lower-tropospheric VWS. More broadly, all quadrants showed that CAPE values tended to decrease, while CIN values were either associated with no significant changes or a shift towards larger magnitudes during the extratropical phase. The rate at which these parameters changed was dependent on the shear-relative location of each quadrant, potentially due to differences in the timing at which each quadrant encountered cooler, drier air. Specifically, the left-of-shear quadrants which were often on the north side of the TC experienced this cooling and drying at an earlier point in transition than the right-of-shear quadrants. Additionally, all quadrants experienced drying throughout the troposphere, however the upshear quadrants experienced stronger drying than their downshear counterparts.

Kinematic environments became more favorable for tornadoes in the right-of-shear quadrants at the beginning of transition. In these quadrants, both the radial and tangential components of winds increased in magnitude from the tropical phase to the transition phase in association with significant increases in SRH. The downshear right quadrant remained most favorable for tornadoes regardless of phase despite tangential winds decreasing in the extratropical phase and small reductions in SRH yielding less

favorable conditions for tornadoes. The left-of-shear quadrants showed insignificant shifts in SRH towards greater magnitudes between the tropical and extratropical phase but did see the same initial increase in the radial and tangential components of the winds followed by a decrease into the extratropical phase.

In summary, extratropical transition is associated with changes to the TC and its synoptic-scale environment, which cause changes to the convective-scale environment in which TC tornadoes are produced. This becomes evident in revisiting the research questions posed in the Introduction:

1. Does the location, timing, frequency, or damage rating of TC tornadoes change as the TC undergoes extratropical transition?

   Yes, tornadoes occur increasingly farther north in the continental United States, while becoming confined to the downshear right quadrant of the TC as transition progresses. Tornadoes also tend to occur later in the day albeit at reduced frequencies, while likely being associated with greater damage ratings during and following transition.

2. How do synoptic-scale characteristics of the TC that could impact tornado occurrence change as the TC undergoes extratropical transition?

   Besides the general asymmetries caused by the interaction of the TC with the baroclinic zone, the outer wind field broadens during transition while TC intensity weakens. These decreases in TC intensity are associated with increased VWS, which becomes more strongly concentrated from the southwest.

3. How do the convective-scale environments in which TC tornadoes are produced change as the TC undergoes extratropical transition?

   As transition completes, all quadrants become less favorable for tornado production. However, the downshear right quadrant remains the most favorable

throughout all phases. In this quadrant, the kinematic and thermodynamic parameters shown in this study either remain the same or become more favorable as transition begins and are least favorable following transition.

The climatology created in this study could be beneficial to forecasters to understand where and when tornadoes are likely to occur based upon the stage of TC transition. This is especially important since TC tornado forecasting is less skillful at all lead times compared to non-TC tornado environments (Edwards 2012; Martinaitis 2017). This study provides needed context to the results of Hill et al. (1966), which also showed a southward progression in TC tornado occurrence. Additionally, this study provides further insight and understanding into how extratropical transition impacts TCs and their embedded convective-scale environments. Specifically, this is the first climatological radiosonde study of the thermodynamic and kinematic structure of extratropically transitioning TCs. Previous work has looked into how VWS, outer size, and distance from the coast impact TC tornado occurrence (Schenkel et al. 2020; Paredes et al. 2021; Schenkel et al. 2021). Nonetheless, this study ties this work together by looking at those characteristics through the frame of extratropical transition, as each of those factors is important during transition.

Future work is necessary to obtain a more complete understanding of how extratropical transition impacts convective-scale environments associated with TC tornadoes. Specifically, these results have raised the following questions:

1. Which process is most important to the enhancement of TC winds and helicity in the downshear right quadrant?

2. Why does tornado occurrence become later as extratropical transition progresses and which processes drive these changes?

3. What processes are most important in causing TC tornadoes to occur increasingly downshear right through transition?

Answers to these questions as well as others could be obtained by computing vorticity budgets and trajectories from simulations of extratropically transitioning TCs with tornadic supercells. Additionally, model-derived soundings could be utilized to examine tornadic supercell proximity soundings, which is not possible with the observed radiosonde data used in this study. To further build upon these results, future work should examine the evolution of TC convection through extratropical transition using radar data.

Reference List

Baker, A. K., M. D. Parker, and M. D. Eastin, 2009: Environmental ingredients for supercells and tornadoes within Hurricane Ivan. *Wea. Forecasting*, **24**, 223–244.

Bian, G.-F., G.-Z. Nie, and X. Qiu, 2021: How well is outer tropical cyclone size represented in the ERA5 reanalysis dataset? *Atmos. Res.*, **249**, 105 339.

Bieli, M., S. J. Camargo, A. H. Sobel, J. L. Evans, and T. Hall, 2019: A global climatology of extratropical transition. Part I: Characteristics across basins. *J. Climate*, **32**, 3557–3582.

Black, M., J. Gamache, F. Marks, C. Samsury, and H. Willoughby, 2002: Eastern Pacific Hurricanes Jimena of 1991 and Olivia of 1994: The effect of vertical shear on structure and intensity. *Mon. Wea. Rev.*, **130**, 2291–2312.

Brammer, A., and C. D. Thorncroft, 2017: Spatial and temporal variability of the three-dimensional flow around African easterly waves. *Mon. Wea. Rev.*, **145**, 2879–2895.

Bunkers, M. J., D. A. Barber, R. L. Thompson, R. Edwards, and J. Garner, 2014: Choosing a universal mean wind for supercell motion prediction. *J. Operat. Meteor.*, **2 (11)**, 115–129.

Corbosiero, K., and J. Molinari, 2003: The relationship between storm motion, vertical wind shear, and convective asymmetries in tropical cyclones. *J. Atmos. Sci.*, **60**, 366–376.

Davies, J., 1990: Midget supercell spawns tornadoes. *Weatherwise*, **43**, 260–260.

Davis, C., C. Snyder, and A. C. Didlake, 2008: A vortex-based perspective of eastern Pacific tropical cyclone formation. *Mon. Wea. Rev.*, **136**, 2461–2477.

Davis, C. A., and L. F. Bosart, 2004: The TT problem: Forecasting the tropical transition of cyclones. *Bull. Amer. Meteor. Soc.*, **85**, 1657–1662.

Ditchek, S. D., K. L. Corbosiero, R. G. Fovell, and J. Molinari, 2020: Electrically active diurnal pulses in Hurricane Harvey (2017). *Mon. Wea. Rev.*, **148**, 2283–2305.

Ditchek, S. D., J. Molinari, K. L. Corbosiero, and R. G. Fovell, 2019: An objective climatology of tropical cyclone diurnal pulses in the Atlantic basin. *Mon. Wea. Rev.*, **147**, 591–605.

Dunion, J. P., C. D. Thorncroft, and C. S. Velden, 2014: The tropical cyclone diurnal cycle of mature hurricanes. *Mon. Wea. Rev.*, **142**, 3900–3919.

Duran, P., and J. Molinari, 2016: Upper-tropospheric low Richardson number in tropical cyclones: Sensitivity to cyclone intensity and the diurnal cycle. *J. Atmos. Sci.*, **73**, 545–554.

Durre, I., R. S. Vose, and D. B. Wuertz, 2006: Overview of the integrated global radiosonde archive. *J. Climate*, **19**, 53–68.

Eastin, M. D., and M. C. Link, 2009: Miniature supercells in an offshore outer rainband of Hurricane Ivan (2004). *Mon. Wea. Rev.*, **137**, 2081–2104.

Edwards, R., 2012: Tropical cyclone tornadoes: A review of knowledge in research and prediction. *Electron. J. Severe Storms Meteor.*, **7**, 1–61.

Edwards, R., and R. M. Mosier, 2022: Over A Quarter Century of TCTOR: Tropical Cyclone Tornadoes in the WSR-88D Era. *Proc., 30th Conf. on Severe Local Storms*, Santa Fe, NM, Amer. Meteor. Soc., 171.

Evans, C., and R. Hart, 2008: Analysis of the wind field evolution associated with the extratropical transition of Bonnie (1998). *Mon. Wea. Rev.*, **136**, 2047–2065.

Evans, C., and Coauthors, 2017: The extratropical transition of tropical cyclones. Part I: Cyclone evolution and direct impacts. *Mon. Wea. Rev.*, **145**, 4317–4344.

Evans, J., and R. Hart, 2003: Objective indicators of the life cycle evolution of extratropical transition for Atlantic tropical cyclones. *Mon. Wea. Rev.*, **131**, 909–925.

Fernández-Cabán, P. L., and Coauthors, 2019: Observing Hurricane Harvey's eyewall at landfall. *Bull. Amer. Meteor. Soc.*, **100**, 759–775.

Franklin, J. L., S. J. Lord, S. E. Feuer, and F. D. Marks, 1993: The kinematic structure of Hurricane Gloria (1985) determined from nested analyses of dropwindsonde and Doppler radar data. *Mon. Wea. Rev.*, **121**, 2433–2451.

Gal-Chen, T., and R. C. Somerville, 1975: On the use of a coordinate transformation for the solution of the Navier-Stokes equations. *J. Comput. Phys.*, **17**, 209–228.

Galarneau, T. J., and C. A. Davis, 2013: Diagnosing forecast errors in tropical cyclone motion. *Mon. Wea. Rev.*, **141**, 405–430.

Gentry, R. C., 1983: Genesis of tornadoes associated with hurricanes. *Mon. Wea. Rev.*, **111**, 1793–1805.

Gilford, D. M., S. Solomon, and K. A. Emanuel, 2017: On the Seasonal Cycles of Tropical Cyclone Potential Intensity. *J. Climate*, **30**, 6085–6096.

Hart, R., 2003: A cyclone phase space derived from thermal wind and thermal asymmetry. *Mon. Wea. Rev.*, **131**, 585–616.

Hart, R., and J. Evans, 2001: A climatology of the extratropical transition of Atlantic tropical cyclones. *J. Climate*, **14**, 546–564.

Hart, R. E., J. L. Evans, and C. Evans, 2006: Synoptic composites of the extratropical transition life cycle of North Atlantic tropical cyclones: Factors determining posttransition evolution. *Mon. Wea. Rev.*, **134**, 553–578.

Hersbach, H., and Coauthors, 2020: The ERA5 global reanalysis. *Quart. J. Roy. Meteor. Soc.*, **146**, 1999–2049.

Hill, E., W. Malkin, and W. Schulz, 1966: Tornadoes associated with cyclones of tropical origin—Practical features. *J. Appl. Meteor. Climatol.*, **5**, 745–763.

Hodges, K., A. Cobb, and P. L. Vidale, 2017: How well are tropical cyclones represented in reanalysis datasets? *J. Climate*, **30**, 5243–5264.

Jones, S., 1995: The evolution of vortices in vertical shear. Part I: Initially barotropic vortices. *Quart. J. Roy. Meteor. Soc.*, **121**, 821–851.

Jones, S. C., and Coauthors, 2003: The extratropical transition of tropical cyclones: Forecast challenges, current understanding, and future directions. *Wea. Forecasting*, **18**, 1052–1092.

Klein, P., P. Harr, and R. Elsberry, 2000: Extratropical transition of western North Pacific tropical cyclones: An overview and conceptual model of the transformation stage. *Wea. Forecasting*, **15**, 373–395.

Landsea, C. W., and J. L. Franklin, 2013: Atlantic hurricane database uncertainty and presentation of a new database format. *Mon. Wea. Rev.*, **141**, 3576–3592.

Marchok, T. P., 2002: How the NCEP Tropical Cyclone Tracker Works. *25th Conf. on Hurricanes and Tropical Meteorology*, San Diego, CA, Amer. Meteor. Soc.

Martinaitis, S. M., 2017: Radar observations of tornado-warned convection associated with tropical cyclones over Florida. *Wea. Forecasting*, **32**, 165–186.

McCaul, E. W., 1991: Buoyancy and shear characteristics of hurricane-tornado environments. *Mon. Wea. Rev.*, **119**, 1954–1978.

McCaul, E. W., D. E. Buechler, S. J. Goodman, and M. Cammarata, 2004: Doppler radar and lightning network observations of a severe outbreak of tropical cyclone tornadoes. *Mon. Wea. Rev.*, **132**, 1747–1763.

McCaul, E. W., and M. L. Weisman, 1996: Simulations of shallow supercell storms in landfalling hurricane environments. *Mon. Wea. Rev.*, **124**, 408–429.

McTaggart-Cowan, R., G. Deane, L. Bosart, C. Davis, and T. Galarneau, 2008: Climatology of tropical cyclogenesis in the North Atlantic (1948-2004). *Mon. Wea. Rev.*, **136**, 1284–1304.

Molinari, J., D. M. Romps, D. Vollaro, and L. Nguyen, 2012: CAPE in tropical cyclones. *J. Atmos. Sci.*, **69**, 2452–2463.

Molinari, J., and D. Vollaro, 2008: Extreme helicity and intense convective towers in Hurricane Bonnie. *Mon. Wea. Rev.*, **136**, 4355–4372.

Molinari, J., and D. Vollaro, 2010: Distribution of helicity, CAPE, and shear in tropical cyclones. *J. Atmos. Sci.*, **67**, 274–284.

Novlan, D. J., and W. M. Gray, 1974: Hurricane-spawned tornadoes. *Mon. Wea. Rev.*, **102**, 476–488.

Paredes, M., B. A. Schenkel, R. Edwards, and M. Coniglio, 2021: Tropical cyclone outer size impacts the number and location of tornadoes. *Geophys. Res. Lett.*, **48**, e2021GL095 922.

Parker, M. D., 2014: Composite VORTEX2 supercell environments from near-storm soundings. *Mon. Wea. Rev.*, **142**, 508–529.

Quinting, J. F., and S. C. Jones, 2016: On the impact of tropical cyclones on rossby wave packets: A climatological perspective. *Mon. Wea. Rev.*, **144**, 2021–2048.

Rios-Berrios, R., and R. D. Torn, 2017: Climatological analysis of tropical cyclone intensity changes under moderate vertical wind shear. *Mon. Wea. Rev.*, **145**, 1717–1738.

Rios-Berrios, R., R. D. Torn, and C. A. Davis, 2016a: An ensemble approach to investigate tropical cyclone intensification in sheared environments. Part I: Katia (2011). *J. Atmos. Sci.*, **73**, 71–93.

Rios-Berrios, R., R. D. Torn, and C. A. Davis, 2016b: An ensemble approach to investigate tropical cyclone intensification in sheared environments. Part II: Ophelia (2011). *J. Atmos. Sci.*, **73**, 1555–1575.

Romps, D. M., and Z. Kuang, 2011: A transilient matrix for moist convection. *J. Atmos. Sci.*, **68**, 2009–2025.

Sarro, G., and C. Evans, 2022: An Updated Investigation of Post-Transformation Intensity, Structural, and Duration Extremes for Extratropically Transitioning North Atlantic Tropical Cyclones. *Mon. Wea. Rev.*, **150**, 2911–2933.

Schenkel, B. A., M. Coniglio, and R. Edwards, 2021: How does the relationship between ambient deep-tropospheric vertical wind shear and tropical cyclone tornadoes change between coastal and inland environments? *Wea. Forecasting*, **36**, 539–566.

Schenkel, B. A., R. Edwards, and M. Coniglio, 2020: A climatological analysis of ambient deep-tropospheric vertical wind shear impacts upon tornadic supercells in tropical cyclones. *Wea. Forecasting*, **35**, 2033–2059.

Schenkel, B. A., and R. Hart, 2012: An examination of tropical cyclone position, intensity, and intensity life cycle within atmospheric reanalysis datasets. *J. Climate*, **25**, 3453–3475.

Schenkel, B. A., N. Lin, D. Chavas, M. Oppenheimer, and A. Brammer, 2017: Evaluating outer tropical cyclone size in reanalysis datasets using QuikSCAT data. *J. Climate*, **30**, 8745–8762.

Schultz, L. A., and D. J. Cecil, 2009: Tropical cyclone tornadoes, 1950–2007. *Mon. Wea. Rev.*, **137**, 3471–3484.

Shapiro, M. A., and D. Keyser, 1990: Fronts, jet streams and the tropopause. *Extratropical cyclones*, Springer, 167–191.

Spratt, S. M., D. W. Sharp, P. Welsh, A. Sandrik, F. Alsheimer, and C. Paxton, 1997: A WSR-88D assessment of tropical cyclone outer rainband tornadoes. *Wea. Forecasting*, **12**, 479–501.

Stern, D. P., G. H. Bryan, and S. D. Aberson, 2016: Extreme low-level updrafts and wind speeds measured by dropsondes in tropical cyclones. *Mon. Wea. Rev.*, **144**, 2177–2204.

Tang, B., and K. Emanuel, 2010: Midlevel ventilation's constraint on tropical cyclone intensity. *J. Atmos. Sci.*, **67**, 1817–1830.

Thorncroft, C., B. Hoskins, and M. McIntyre, 1993: Two paradigms of baroclinic-wave life-cycle behaviour. *Quart. J. Roy. Meteor. Soc.*, **119**, 17–55.

Torn, R. D., and C. Snyder, 2012: Uncertainty of tropical cyclone best-track information. *Wea. Forecasting*, **27**, 715–729.

Wang, J., and Coauthors, 2015: A long-term, high-quality, high-vertical-resolution GPS dropsonde dataset for hurricane and other studies. *Bull. Amer. Meteor. Soc.*, **96**, 961–973.

Wessel, P., and W. H. Smith, 1996: A global, self-consistent, hierarchical, high-resolution shoreline database. *J. Geophys. Res.*, **101**, 8741–8743.